



Understanding the treatment of waves in atmospheric models, Part I: The shortest resolved waves of the 1D linearized shallow water equations

P. A. Ullrich*

*Correspondence to: Paul Ullrich, Department of Land, Air and Water Resources, University of California, Davis, One Shields Ave., Davis, CA 95616. Email: paulullrich@ucdavis.edu

This paper provides an intercomparison of the dispersive and diffusive properties of several standard numerical methods applied to the 1D linearized shallow water equations without Coriolis term, including upwind and central finite-volume, spectral finite-volume, discontinuous Galerkin, spectral element, and staggered finite-volume. All methods are studied up to tenth-order accuracy, where possible. A consistent framework is developed which allows for direct intercomparison of the ability of these methods to capture the behavior of linear gravity waves. The Courant-Friedrichs-Lewy (CFL) condition is also computed, which is important for gauging the stability of these methods, and leads to a measure of approximate equal error cost. The goal of this work is threefold: first, to determine the shortest wavelength which can be considered “resolved” for a particular method; second, to determine the effect of increasing the order of accuracy on the ability of a method to capture wave-like motion; third, to determine which numerical methods offer the best treatment of wave-like motion. Copyright © 2012 Royal Meteorological Society

Key Words: High-order; dispersion analysis; finite-volume methods; finite-element methods; linear gravity waves; dynamical core

Received ...

Citation: ...

1. Introduction

To a close approximation, the atmosphere is in a state of geostrophic and hydrostatic balance. The dynamic character of the atmosphere is governed by a slow adjustment process which gives rise to wave motion over all scales. Accurate treatment of these waves is important to capture departures from geostrophic balance, and to ensure that the adjustment process is correct and free from spurious numerical errors. As shown by [Lauritzen *et al.* \(2010\)](#), an accurate treatment of the equations of motion is also important to avoid errors due to grid imprinting. The capability of a numerical method to capture wave-like motion in atmospheric models is typically evaluated using dispersion analysis ([Randall 1994](#)). This mathematical technique decomposes the discrete response in the atmospheric model into diffusive and dispersive errors introduced by the discretization. Diffusive errors are

typically associated with an unphysical loss of wave energy from the system and dispersive errors are associated with an incorrect treatment of individual wave speeds which can lead to unphysical ringing or incorrect wave packet velocity.

This paper is the first in a series aimed at better understanding the wave structure of numerical methods of arbitrary order-of-accuracy. Although previous efforts ([Lauritzen 2007](#); [Skamarock 2008](#); [Thuburn 2008](#); [Thuburn *et al.* 2009](#)) have been effective at understanding the dispersive behavior of particular, generally low-order, numerical discretizations of the 1D wave equation, this work aims to provide a consistent framework for the intercomparison of the dispersive properties of many standard numerical methods of all orders of accuracy. Specifically, this paper aims to answer four questions:

- What are the shortest waves which can be considered “resolved” for a particular numerical method?

- What is the effect of increasing the order of accuracy of a numerical discretization on its treatment of waves?
- For a given order of accuracy, which numerical methods offer the best treatment of wave-like motion?
- For a given error level, which numerical method and order of accuracy is the most computationally efficient?

Along with method-specific papers, which are presented along with the model formulation in section 3, dispersion analysis has been a major focus in the literature. However, to the best of the author's knowledge, no other work has presented a comprehensive intercomparison of the dispersion properties of standard numerical methods. Specifically, this paper includes an analysis of unstaggered and staggered finite-volume methods, plus popular compact schemes such as spectral element, discontinuous Galerkin and spectral finite-volume.

The structure of this paper is as follows. In section 2 a framework is presented which allows for consistent expression of a wide class of numerical methods, along with the methodology for performing linear dispersion analysis in this framework. The results of dispersion analysis for eight numerical methods up to tenth-order accuracy are presented in section 3 along with a brief discussion of how to formulate each method. Further discussion and intercomparison of the results of the analysis are presented in section 4. Conclusions and future work are given in section 5.

2. Methodology

2.1. Discretization of the continuous equations

The 1D linearized shallow water equations can be written as a coupled system of differential equations,

$$\frac{\partial u}{\partial t} + \frac{\partial \Phi}{\partial x} = 0, \quad (1)$$

$$\frac{\partial \Phi}{\partial t} + \Phi_0 \frac{\partial u}{\partial x} = 0, \quad (2)$$

where $u(x, t)$ is the 1D linear velocity in the x direction, $\Phi(x, t) = gh(x, t)$ is the perturbed geopotential, where $h(x, t)$ is the perturbation in the height of the fluid above some surface $z = z_0$ and $\Phi_0 = gz_0$. The acceleration due to gravity g is assumed constant.

The 1D real line is divided into elements of width Δx_e which bound the range $[j\Delta x_e, (j+1)\Delta x_e]$, with index $j \in \mathbb{Z}$. An Eulerian discretization of (1)-(2) which stores m degrees-of-freedom (DOFs) per variable per element has a discrete state vector $\mathbf{q}_j = \{\mathbf{u}_j, \Phi_j\}$ associated with each element of the form

$$\mathbf{u}_j = \{u_{j,1}, \dots, u_{j,m}\}, \quad (3)$$

$$\Phi_j = \{\Phi_{j,1}, \dots, \Phi_{j,m}\}. \quad (4)$$

Assuming that the spatial discretization is homogeneous and linear, the semi-discrete evolution equations can then

be written as

$$\frac{\partial \mathbf{u}_j}{\partial t} + \frac{1}{\Delta x_e} \sum_{\ell=-N_g}^{N_g} \mathbf{A}^{(\ell)} \Phi_{j+\ell} = \frac{\sqrt{\Phi_0}}{\Delta x_e} \sum_{\ell=-N_g}^{N_g} \mathbf{C}^{(\ell)} \mathbf{u}_{j+\ell}, \quad (5)$$

$$\frac{\partial \Phi_j}{\partial t} + \frac{\Phi_0}{\Delta x_e} \sum_{\ell=-N_g}^{N_g} \mathbf{B}^{(\ell)} \mathbf{u}_{j+\ell} = \frac{\sqrt{\Phi_0}}{\Delta x_e} \sum_{\ell=-N_g}^{N_g} \mathbf{D}^{(\ell)} \Phi_{j+\ell}. \quad (6)$$

Here N_g denotes the girth of the semi-discrete stencil, defined as $N_g = (N_s - 1)/2$ where N_s is the total stencil size and Δx_e is the element width. Associated with the element width is the average distance between degrees of freedom, $\Delta x = \Delta x_e/m$, which is a consistent measure of grid spacing between numerical methods. The unitless matrices $\mathbf{A}^{(\ell)}$ and $\mathbf{B}^{(\ell)}$ represent the discrete *advective* term, whereas the unitless matrices $\mathbf{C}^{(\ell)}$ and $\mathbf{D}^{(\ell)}$ include effects due to *numerical diffusion* which arises from the formulation of the method. Namely, $\mathbf{C}^{(\ell)}$ and $\mathbf{D}^{(\ell)}$ encapsulate numerical diffusion which is either associated with an explicit diffusion operator or which arises from use of a Riemann solver, and should not be confused with diffusion due to truncation error. For consistency with (1)-(2) the following conditions must also be satisfied for a numerical method of order p :

$$\frac{1}{\Delta x_e} \sum_{\ell=-N_g}^{N_g} \mathbf{A}^{(\ell)} \Phi_{j+\ell} = \frac{\partial \Phi}{\partial x} \Big|_{\mathbf{x}=\mathbf{x}_j} + \mathcal{O}(\Delta x_e^p), \quad (7)$$

$$\frac{1}{\Delta x_e} \sum_{\ell=-N_g}^{N_g} \mathbf{B}^{(\ell)} \mathbf{u}_{j+\ell} = \frac{\partial u}{\partial x} \Big|_{\mathbf{x}=\mathbf{x}_j} + \mathcal{O}(\Delta x_e^p), \quad (8)$$

$$\frac{1}{\Delta x_e} \sum_{\ell=-N_g}^{N_g} \mathbf{C}^{(\ell)} \mathbf{u}_{j+\ell} = \mathcal{O}(\Delta x_e^p), \quad (9)$$

$$\frac{1}{\Delta x_e} \sum_{\ell=-N_g}^{N_g} \mathbf{D}^{(\ell)} \Phi_{j+\ell} = \mathcal{O}(\Delta x_e^p), \quad (10)$$

where \mathbf{x}_j denotes the point (or cell) where the state variable Φ_j or u_j is defined.

If the $\mathbf{A}^{(\ell)} = \mathbf{B}^{(\ell)}$ and $\mathbf{C}^{(\ell)} = \mathbf{D}^{(\ell)}$, then (5)-(6) can be condensed into an uncoupled system of two linear advection equations. Namely, if we define the right-going Riemann invariant $\mathbf{R}_j = \Phi_j + \sqrt{\Phi_0} \mathbf{u}_j$ and left-going invariant $\mathbf{L}_j = \Phi_j - \sqrt{\Phi_0} \mathbf{u}_j$, it then follows that (5)-(6) is equivalent to the decoupled system of advection equations

$$\frac{\partial \mathbf{L}_j}{\partial t} - \frac{\sqrt{\Phi_0}}{\Delta x_e} \sum_{\ell=-N_g}^{N_g} (\mathbf{A}^{(\ell)} + \mathbf{C}^{(\ell)}) \mathbf{L}_{j+\ell} = 0, \quad (11)$$

$$\frac{\partial \mathbf{R}_j}{\partial t} + \frac{\sqrt{\Phi_0}}{\Delta x_e} \sum_{\ell=-N_g}^{N_g} (\mathbf{A}^{(\ell)} - \mathbf{C}^{(\ell)}) \mathbf{R}_{j+\ell} = 0. \quad (12)$$

Unstaggered numerical discretizations typically satisfy this property, and consequently dispersion analysis of the linearized shallow water equations is greatly simplified for these methods.

2.2. Dispersion analysis

The discrete evolution equations (5)-(6) can be written in matrix notation as

$$\frac{\partial}{\partial t} \begin{pmatrix} \mathbf{u} \\ \Phi \end{pmatrix}_j = \sum_{\ell=-N_g}^{N_g} \frac{1}{\Delta x_e} \underbrace{\begin{pmatrix} \sqrt{\Phi_0} C^{(\ell)} & -A^{(\ell)} \\ -\Phi_0 B^{(\ell)} & \sqrt{\Phi_0} D^{(\ell)} \end{pmatrix}}_{\equiv M^{(\ell)}} \begin{pmatrix} \mathbf{u} \\ \Phi \end{pmatrix}_{j+\ell} \quad (13)$$

Now, consider a single element-wise wave mode of the form

$$\begin{pmatrix} \mathbf{u}(t) \\ \Phi(t) \end{pmatrix}_j = \begin{pmatrix} \mathbf{u}_{k_e}(t) \\ \Phi_{k_e}(t) \end{pmatrix}_0 \exp(ij\theta_e), \quad (14)$$

with dimensionless wavenumber $\theta_e \in [0, 2\pi)^*$, element-wise wavenumber $k_e = \theta_e / \Delta x_e$ and wavelength $\lambda_e = 2\pi / k_e$. The subscript k_e here denotes that only a single element-wise wavenumber is being captured. Following (13), this mode evolves according to

$$\frac{\partial}{\partial t} \begin{pmatrix} \mathbf{u}_{k_e}(t) \\ \Phi_{k_e}(t) \end{pmatrix}_0 = \underbrace{\left(\sum_{\ell=-N_g}^{N_g} M^{(\ell)} \exp(i\ell\theta_e) \right)}_{\equiv M_{k_e}} \begin{pmatrix} \mathbf{u}_{k_e}(t) \\ \Phi_{k_e}(t) \end{pmatrix}_0 \quad (15)$$

The linear frequency ω of this wave mode is defined via

$$\begin{pmatrix} \mathbf{u}_{k_e}(t) \\ \Phi_{k_e}(t) \end{pmatrix}_0 = \begin{pmatrix} \tilde{\mathbf{u}}_{k_e} \\ \tilde{\Phi}_{k_e} \end{pmatrix}_0 \exp(-i\omega t), \quad (16)$$

in which case (15) satisfies

$$\omega \begin{pmatrix} \tilde{\mathbf{u}}_{k_e} \\ \tilde{\Phi}_{k_e} \end{pmatrix}_0 = iM_{k_e} \begin{pmatrix} \tilde{\mathbf{u}}_{k_e} \\ \tilde{\Phi}_{k_e} \end{pmatrix}_0. \quad (17)$$

This equation describes the behavior of wave modes of the numerical discretization under exact time integration. Observe that ω is an eigenvalue of the matrix iM_{k_e} , and so takes on values $\omega^{(1)}, \dots, \omega^{(m)}$, which corresponds to m distinct waves. Consequently, the matrix iM_{k_e} , via its eigenvectors and eigenvalues, encodes all information about the natural modes of oscillation of the discretization and their corresponding frequency and growth rate. For a given complex eigenvalue $\omega^{(p)}$ of iM_{k_e} , with complex decomposition $\omega^{(p)} = \omega_r^{(p)} + i\omega_i^{(p)}$ the oscillation frequency of the wave mode is $\omega_r^{(p)}$ and the growth rate is $\omega_i^{(p)}$. The growth rate corresponds to an *amplification factor* associated with a particular wave mode equal to

$$|A|_k = \exp(\omega_i^{(p)} \Delta x / \sqrt{\Phi_0}). \quad (18)$$

Here, $|A|_k$ represents the degree of amplification experienced by the wave after one characteristic unit of time $t_c = \Delta x / \sqrt{\Phi_0}$. This normalization ensures that the effect

*In total, a numerical discretization on a mesh of N_e elements will resolve N_e real modes with $\theta_e = \pi j / N_e$ for integer index $j \in [0, N_e - 1]$. The range $[\pi, 2\pi)$ is associated with the complex conjugate of the resolved modes. Note that this arrangement implies that half of the total storage requirement is associated with wave modes of $4\Delta x$ or shorter.

of amplification on a wave is measured independent of the choice of Courant number. The subscript k denotes that a single wave (among the m element-wise waves) is being captured.

If the numerical discretization is unstaggered with evolution equation (12), the same analysis can be performed under the construction

$$\mathbf{R}_j = \mathbf{R}_0 \exp(i(j\theta_e - \omega t)), \quad (19)$$

which leads to

$$\omega \mathbf{R}_0 = -i \underbrace{\left(\sum_{\ell=-N_g}^{N_g} \frac{\sqrt{\Phi_0}}{\Delta x_e} (A^{(\ell)} - C^{(\ell)}) \exp(i\ell\theta_e) \right)}_{\equiv iM_{k_e}} \mathbf{R}_0. \quad (20)$$

Note that for unstaggered discretizations, the nature of $A^{(\ell)}$ as a discretization of the undamped wave operator suggests that the matrix

$$A_{k_e} \equiv \sum_{\ell=-N_g}^{N_g} A^{(\ell)} \exp(ij\theta_e) \quad (21)$$

will have purely imaginary eigenvalues for all possible values of θ_e , and hence as a standalone operator conserves linear wave energy. Analogously, from the nature of $C^{(\ell)}$ as a diffusion operator, the matrix

$$C_{k_e} \equiv \sum_{\ell=-N_g}^{N_g} C^{(\ell)} \exp(ij\theta_e) \quad (22)$$

should have purely real eigenvalues. The matrices A_{k_e} and C_{k_e} retain these properties for all numerical methods examined herein, but it remains fairly easy to construct a stable, convergent numerical method for which A_{k_e} has complex eigenvalues (see, for example, [Van den Abeele et al. \(2007\)](#)).

2.3. Analysis of compact schemes

Several of the methods in this paper are *compact*, meaning that each element only needs to communicate with its immediate neighbors (in terms of the notation in (5)-(6), this implies $N_g = 1$). Compact schemes are particularly desirable for use on large-scale parallel systems since they tend to have nearly optimal parallel scalability. For the compact schemes considered in this paper, the DOFs of each element are interpreted as the weights of a corresponding set of compact basis functions on a reference element $\xi \in [0, 1]$, denoted by $\hat{u}_i(\xi)$ and $\hat{\Phi}_i(\xi)$. Consequently, they induce the continuous extension of the discrete state,

$$\hat{u}(x) = \sum_{j=-\infty}^{\infty} \sum_{i=1}^m u_{j,i} \hat{u}_i(x/\Delta x_e - j), \quad (23)$$

$$\hat{\Phi}(x) = \sum_{j=-\infty}^{\infty} \sum_{i=1}^m \Phi_{j,i} \hat{\Phi}_i(x/\Delta x_e - j). \quad (24)$$

Note that the compact basis functions can extend beyond the interval $\xi \in [0, 1]$, such as in the case of spectral element methods.

The dimensionless wavenumber θ_e spans the range $[0, 2\pi)$, where each value θ_e is associated with m distinct eigenvectors. In the previous section it was demonstrated that on an element-wise level, linear numerical discretizations of the linearized shallow water equations support wave modes (associated with a unique dimensionless wavenumber) which are decoupled from all others. However, if nodal degrees of freedom are non-uniformly distributed within an element (as with any of the compact numerical schemes discussed herein), this result will not hold on a nodal level. That is, the natural modes of oscillation of the numerical discretization cannot necessarily be characterized as wave-like.[†] Nonetheless, one does expect that these modes do exhibit approximately wave-like character, especially for long waves. This observation motivates the following definition:

Definition 1: The *approximate dimensionless wavenumber* $\theta \in [0, 2\pi)$ associated with wavenumber θ_e and eigenvector / eigenvalue pair $(\mathbf{q}^{(p)}, \omega^{(p)})$ is the value $\theta^{(p)} = (\theta_e + 2\pi n)/m$ for integer $0 \leq n < m$ that maximizes

$$\left| \int_0^1 \left[\hat{\Phi}(\xi) + \sqrt{\Phi_0} \hat{u}(\xi) \right] \exp(-im\theta^{(p)}\xi) d\xi \right|, \quad (25)$$

where the coefficients of $\hat{\Phi}(x)$ and $\hat{u}(x)$ are determined by $\mathbf{q}^{(p)}$, and $\lambda_e = 2\pi/k_e$.

The approximate dimensionless wavenumber has wavenumber $k = \theta^{(p)}/\Delta x$, and corresponding wavelength $\lambda = 2\pi/k$. For non-compact schemes it is simply the case that $n = 0$ and $\theta = \theta_e$. Modes with $n > 0$ are sometimes labelled as “spurious modes” or “computational modes” in the literature (see, for example [Hu et al. \(1999\)](#)), however this is arguably an incorrect characterization since these modes correspond to sub-element-scale resolution of physical wave modes.

Once k has been determined for each discrete wave mode, the phase speed c_p and group speed c_g of each wave mode are defined in the usual manner,

$$c_p = \frac{\omega_r}{k}, \quad \text{and} \quad c_g = \frac{\partial \omega_r}{\partial k}, \quad (26)$$

where ω_r is a continuous extension of the set $\omega_r^{(p)}$ over k .

2.4. Effective resolution

Loosely defined, the *effective resolution* of a numerical method is the resolution at which the numerical method can be considered to have accurately resolved the character of the flow. Although waves of wavelength as short as $2\Delta x$ ($\theta = \pi$) can be represented on the discrete grid, the dispersive properties of these short-wavelength modes generally diverge from the exact dispersion relation $\omega = \sqrt{\Phi_0}k$ at much longer wavelengths. To quantify the effective resolution of the scheme, we follow [Hu et al. \(1999\)](#) in proposing the following definitions:

[†] Compact numerical schemes which have a greater density of nodal points near element edges tend to support high-frequency eigenmodes which are concentrated in regions of fine grid spacing. It is for this reason that the CFL condition associated with these methods tends to be more restrictive than approaches which use a uniformly spaced grid.

Definition 2: For a given error level $\tilde{\epsilon}_r$, the *shortest resolved wavelength (dispersive limit)* is the wavelength $\lambda_s = a\Delta x$, such that

$$\left| \omega_r \frac{\Delta x}{\sqrt{\Phi_0}} - \theta \right| \leq \tilde{\epsilon}_r \quad (27)$$

for all waves with wavelength $\lambda \geq \lambda_s$.

Definition 3: For a given error level $\tilde{\epsilon}_i$, the *shortest resolved wavelength (diffusive limit)* is the wavelength $\lambda_s = a\Delta x$, such that

$$\left| \omega_i \frac{\Delta x}{\sqrt{\Phi_0}} \right| \leq \tilde{\epsilon}_i \quad (28)$$

for all waves with wavelength $\lambda \geq \lambda_s$.

Although it may not be clear in practice what minimum standards should be required of a numerical method, this paper makes use of an error level of $\tilde{\epsilon}_r = \tilde{\epsilon}_i = 0.01$. This definition corresponds to the wave being completely out of phase over a distance of $(\pi/0.01)\Delta x$ and to 10% damping of the wave over a distance of approximately $10\Delta x$.

2.5. Maximum Stable Courant number (CFL condition)

An analysis of the relative efficiency of these methods is incomplete without some understanding of how large of a time step can be taken under a corresponding temporal discretization. This work focuses on five common Runge-Kutta methods, which have been chosen due to their robustness when applied to arbitrary spatial discretizations. These include the standard RK2, RK3 and RK4 discretizations, plus the strong-stability preserving five-stage and six-stage third-order Runge-Kutta methods of [Ruuth \(2006\)](#) (SSPRK53 and SSPRK63, respectively). Given the characteristic polynomial $P(x)$ of a Runge-Kutta method, the update equation following from (15) can be written as

$$\begin{pmatrix} \mathbf{u}_k \\ \Phi_k \end{pmatrix}_0^{n+1} = P(\Delta t M_k) \begin{pmatrix} \mathbf{u}_k \\ \Phi_k \end{pmatrix}_0^n. \quad (29)$$

This update equation is then stable in the von Neumann sense if for all $\theta_e \in [0, \pi]$ the matrix $P(\Delta t M_k)$ has eigenvalues p_j which all satisfy $|p_j| \leq 1$. For the linearized shallow water equations, this stability criteria can be formulated as an upper bound on the dimensionless Courant number,

$$C = \frac{\Delta t \sqrt{\Phi_0}}{\Delta x}. \quad (30)$$

In practice, this upper bound for each numerical method is determined via a grid search over the 2D domain $[\theta_e, C]$.

2.6. Approximate equal error cost

The procedure described so far is effective at quantifying the linear dispersive and diffusive error of a particular numerical method as well as the corresponding time step constraints. However, a single metric which accounts for the approximate computational cost required to achieve a particular error level is desirable. To approximate computational cost, the average number of non-zero entries per DOF in the evolution matrices is used, since this

value approximates the number of memory accesses and/or floating point operations needed over one Runge-Kutta stage per DOF. Consequently, if the error rate is fixed and the mesh resolution is allowed to vary, one can define an approximate equal error cost associated with each numerical method and order of accuracy as follows:

$$\begin{aligned} &\langle \text{Approximate equal error cost} \rangle \\ &= \langle \text{Average non-zeros per DOF} \rangle \\ &\quad \times \langle \text{Shortest resolved wavelength} \rangle \\ &\quad \times \langle \text{Number of RK stages per time step} \rangle \\ &\quad / \langle \text{Maximum stable Courant number} \rangle \end{aligned} \quad (31)$$

Here the shortest resolved wavelength refers to the longer wave among the dispersive and diffusive limits. It should be emphasized that the approximate equal error cost is a very rough heuristic measure and does not take into account many issues which will arise in practice, some of which are described in section 2.7: In particular, parallel scalability is not accounted for in this calculation, although it is an important feature for next-generation atmospheric models. Furthermore, methods with no implicit diffusion will exhibit significantly smaller approximate equal error cost, since they do not require evaluation of the numerical diffusion matrices (which will be required in practice).

2.7. Caveats

The linear analysis presented in this work has several important caveats that must be considered in practice:

- The dispersive properties of numerical methods can change drastically depending on the choice of temporal discretization. Although most methods with no implicit diffusion are largely unaffected by this choice, if implicit diffusion is present the phase speed and amplification factor of each wave mode can change drastically as Δt is scaled towards the maximum stable Courant number. Nonetheless, the analysis performed in this work holds in the limit of $\Delta t \rightarrow 0$. Some discussion of this behavior can be found in Ullrich and Jablonowski (2011).
- The addition of explicit diffusion, as is generally needed for schemes with no implicit diffusion and compact schemes of high-order accuracy, will directly influence the amplification factor of all wave modes. The phase speed is also generally affected through the application of explicit diffusion, although to the best of the author's knowledge there are no studies that consider this effect. Some preliminary evidence suggests that diffusion, if added in a time-split manner, may improve the phase capturing properties of numerical methods.
- As noted by Rančić *et al.* (2008) and Thuburn (2011), proper simulation of the nonlinear energy and enstrophy cascade is essential to any long-term integration of the equations of motion. This cascade does not appear in the linear analysis, but it is an important consideration when selecting a numerical method for scientific operation. In particular, whereas the spectral transform method is exact in the linear regime, it is only with the introduction of nonlinearities that this scheme is challenged. How the choice of numerical method affects the behavior of

the energy and enstrophy spectrum remains an open question, and the "correct" mechanism for enforcing diffusion at the smallest scales remains up for debate. Notably, some evidence suggests that treatment of small-scale turbulence may require the addition of parameterizations for backscatter and eddy viscosity (Frederiksen and Davies 1997).

3. Results

The eight spatial discretizations analyzed in this paper are summarized in Table 1. Five of these methods are compact. Seven of these schemes are unstaggered methods, and so can be completely specified via the matrices $A^{(\ell)}$ and $C^{(\ell)}$. Finally, four schemes have matrices M_k with purely imaginary eigenvalues and hence implicitly conserve linear wave energy. In practice, these methods will need some explicitly added diffusion to remove noise from the system.

Using the analysis procedure discussed in section 2, the shortest resolved wave, dispersive limit, diffusive limit and maximum stable Courant number (CFL condition) have been computed for the eight methods introduced in this paper. The shortest resolved wavelength for all schemes of at least second-order accuracy (up to tenth-order accuracy) are plotted in Figure 1. Tabulated results are given in Table 2, for schemes which exhibit implicit diffusion, including UFV, SFV, DG and DG*. Results are given in Table 3 for schemes with no implicit diffusion, including CFV, SEM, MB-SEM and stFV.

The methods in this paper which exhibit implicit diffusion require the use of a Riemann solver to compute fluxes at element edges. The Lax-Friedrichs Riemann solver will be used in this case, which for the linearized shallow water equations take left and right edge values Φ_L , Φ_R , u_L and u_R , and produces velocity and geopotential fluxes given by

$$\hat{F}_u = \frac{1}{2}(\Phi_R + \Phi_L) - \frac{\sqrt{\Phi_0}}{2}(u_R - u_L), \quad (32)$$

$$\hat{F}_\Phi = \frac{\Phi_0}{2}(u_R + u_L) - \frac{\sqrt{\Phi_0}}{2}(\Phi_R - \Phi_L). \quad (33)$$

Other well-known Riemann solvers, including the Roe Riemann solver (Roe 1981) and HLL Riemann solver (Harten *et al.* 1983) yield an identical flux formula for linearized equations.

The remainder of this section provides a discussion of the methods analyzed in this work.

3.1. Upwind/Central Finite-Volume (UFV/CFV) methods

The one-element biased UFV method is based on the first-order upwind scheme of Godunov (1959), and higher-order generalizations (Van Leer 1979). The dispersive properties of these methods have been studied in detail by Li (1997). Upwind finite-volume methods have been implemented in a shallow-water model (Rossmanith 2006; Ullrich *et al.* 2010), as a mesoscale atmospheric model (Ullrich and Jablonowski 2012b) and as a global atmospheric dynamical core (Ullrich and Jablonowski 2012a). In general, UFV methods of this type on a stencil of girth $N_g = (p + 1)/2$ will have an order-of-accuracy of p , under the constraint of p odd. Each element only stores one degree of freedom, given by the element-average within that element. High-order accuracy is obtained via a reconstruction procedure

Table 1. Overview of the numerical methods analyzed in this paper.

Method	Acronym	Compact?	Staggered?	Implicit Diffusion?
Upwind Finite-Volume	UFV	No	No	Yes
Central Finite-Volume	CFV	No	No	No
Spectral Finite-Volume	SFV	Yes	No	Yes
Discontinuous Galerkin	DG	Yes	No	Yes
Mass-Lumped Discontinuous Galerkin	DG*	Yes	No	Yes
Spectral Element Method	SEM	Yes	No	No
Modified-Basis Spectral Element Method	MB-SEM	Yes	No	No
Staggered Finite-Volume	stFV	No	Yes	No

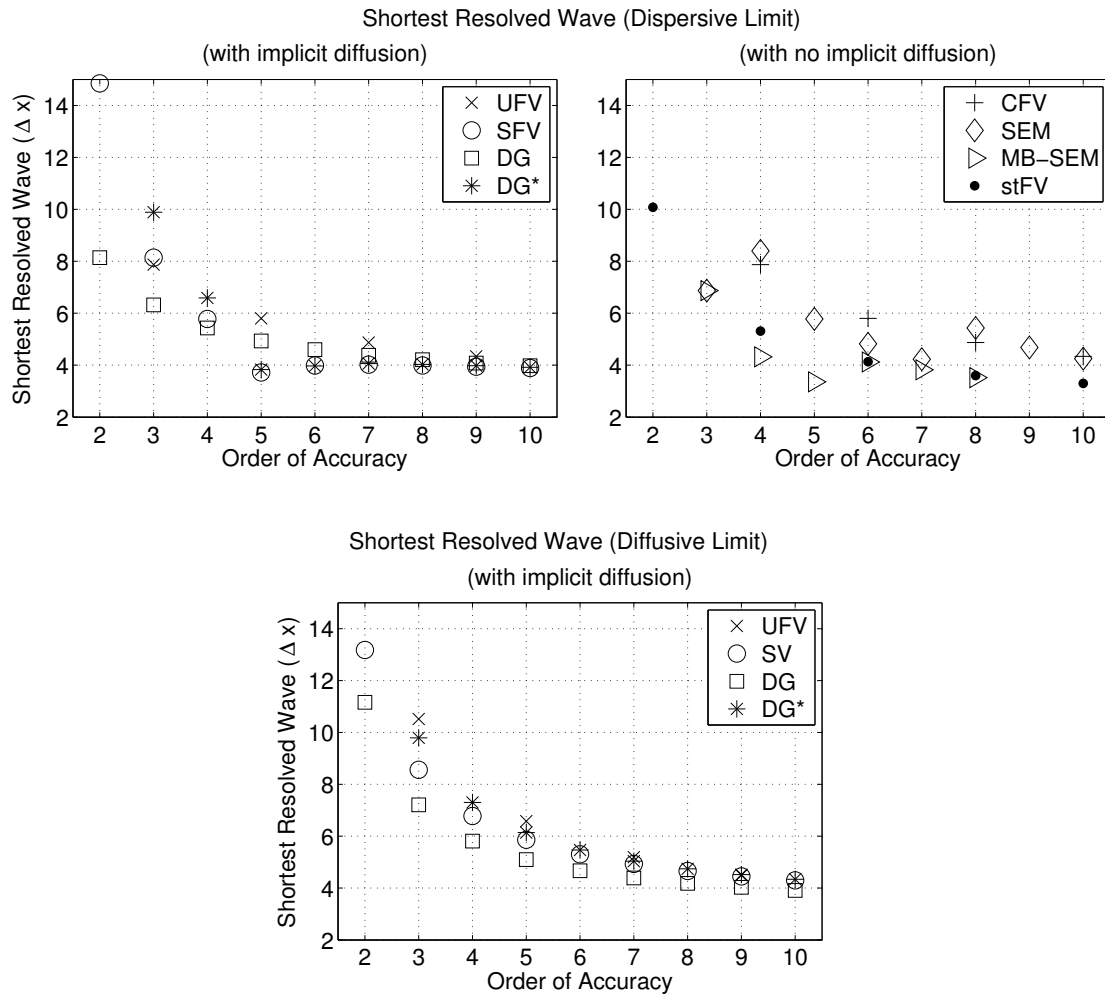


Figure 1. Shortest resolved wavelength in the (top) dispersive limit and (bottom) diffusive limit with error level $\tilde{\epsilon}_r = \tilde{\epsilon}_i = 0.01$ for all methods considered in this paper and order of accuracy ≥ 2 . Only results with a shortest resolved wavelength below $15\Delta x$ are shown.

which uses neighboring information to obtain an accurate approximation to the underlying field.

The central finite-volume method on a stencil of girth $N_g = p/2$ will have an order-of-accuracy of p , where under the constraint of symmetry p must be even. Again, each element has exactly one degree of freedom per state variable which is interpreted as the element average. At second-order accuracy, this method reduces to the well-known central difference method. At fourth-order accuracy, this class of methods includes the piecewise parabolic method of

Colella and Woodward (1984) when the non-linear limiting procedure is not used.

For an arbitrary hyperbolic differential equation, both upwind and central finite-volume methods are constructed as follows:

1. For each edge $j + 1/2$ polynomials $\Phi_L(x)$, $\Phi_R(x)$, $u_L(x)$ and $u_R(x)$ are fit through elements $[j - N_g + 1, \dots, j + N_g - 1]$ and $[j - N_g + 2, \dots, j + N_g]$ such that the element-averages of the polynomial

Table 2. Schemes with implicit diffusion: Shortest resolved wavenumber in the dispersive limit and diffusive limit, maximum stable Courant number and average number of non-zeros per node. These schemes include the Upwind Finite-Volume (UFV), Spectral Element Method (SEM), Spectral Volume (SFV) method and Discontinuous Galerkin (DG) method with RK2, RK3, SSPRK53 and SSPRK63 time-stepping schemes.

Scheme	Order	Shortest Resolved Wavelength		Maximum Stable Courant Number					Non-zeros
		Disp. Limit (Δx)	Diff. Limit (Δx)	RK2	RK3	RK4	SSPRK53	SSPRK63	
UFV	1	16.01	44.39	1.00	1.26	1.39	2.86	3.60	10
	3	7.87	10.52	-	1.63	1.75	2.42	2.73	18
	5	5.80	6.58	-	1.44	1.73	2.08	2.33	26
	7	4.87	5.19	-	1.24	1.69	1.84	2.07	34
	9	4.34	4.49	-	1.13	1.60	1.68	1.90	42
SFV	1	16.01	44.39	1.00	1.26	1.39	2.86	3.60	10
	2	14.85	13.18	1.00	1.19	1.39	2.17	2.56	16
	3	8.14	8.56	-	0.97	1.09	1.79	2.11	17.3
	4	5.78	6.78	-	0.81	0.91	1.54	1.83	19
	5	3.72	5.86	-	0.70	0.78	1.36	1.62	20.8
	6	3.99	5.30	-	0.62	0.69	1.23	1.47	22.7
	7	4.02	4.93	-	0.56	0.62	1.12	1.34	24.6
	8	3.99	4.66	-	0.51	0.57	1.03	1.24	26.5
	9	3.94	4.45	-	0.47	0.53	0.96	1.15	28.4
	10	3.89	4.30	-	0.44	0.49	0.90	1.08	30.4
DG	1	16.01	44.39	1.00	1.26	1.39	2.86	3.60	10
	2	8.14	11.16	0.67	0.82	0.93	1.56	1.86	16
	3	6.32	7.21	-	0.63	0.71	1.22	1.45	17.3
	4	5.43	5.81	-	0.52	0.58	1.02	1.23	19
	5	4.93	5.10	-	0.45	0.50	0.89	1.07	20.8
	6	4.60	4.67	-	0.40	0.44	0.80	0.96	22.7
	7	4.38	4.39	-	0.36	0.40	0.72	0.87	24.6
	8	4.21	4.18	-	0.33	0.36	0.66	0.80	26.5
	9	4.08	4.03	-	0.30	0.33	0.61	0.75	28.4
	10	3.98	3.91	-	0.28	0.31	0.57	0.70	30.4
DG*	1	16.01	44.39	1.00	1.26	1.39	2.86	3.60	10
	2	23.99	17.82	2.00	2.12	2.47	3.61	4.23	8
	3	9.89	9.79	-	1.35	1.54	2.34	2.71	8
	4	6.59	7.30	-	1.02	1.15	1.85	2.16	9
	5	3.83	6.14	-	0.84	0.95	1.57	1.85	10.4
	6	3.97	5.47	-	0.72	0.81	1.38	1.63	12.0
	7	4.06	5.04	-	0.64	0.72	1.24	1.47	13.7
	8	4.03	4.74	-	0.58	0.65	1.13	1.34	15.5
	9	3.98	4.52	-	0.53	0.59	1.04	1.24	17.3
	10	3.92	4.34	-	0.49	0.54	0.97	1.16	19.2

over each element matches the known element-average of that element.

2. The polynomials are evaluated at $x_{j+1/2}$, yielding the reconstructed value of the state variable at the edge $\Phi_L(x_{j+1/2})$, $\Phi_R(x_{j+1/2})$, $u_L(x_{j+1/2})$ and $u_R(x_{j+1/2})$.
3. If upwind finite-volume methods are desired, the flux is calculated via a Riemann solver. If a central finite-volume method is desired, the flux is instead calculated via a central flux (that is, the average of the fluxes on both sides of the volume edge).
4. The element average in cell j is updated in accordance with the flux \hat{F} through edges $j - 1/2$ and $j + 1/2$.

The coefficients of finite-volume methods are given in Table 4 up to schemes of order 9. The coefficients of $A^{(\ell)}$ correspond to even-order central approximations to the advective operator, and are identical for both upwind and central finite-volume methods. The coefficients of $C^{(\ell)}$

are non-zero only for upwind finite-volume methods, in which case they approximate a diffusive operator which is proportional to $\Delta x^{p+1} \nabla^{p+1}$, leading to a scheme which overall is p^{th} -order accurate. The corresponding phase speed and amplification factor are given in Figure 2 up to ninth-order. Worth noting about the finite-volume methods is that the phase speed and amplification factor are decoupled (a property which is not present among the compact family of schemes present in this paper), and so both upwind and central schemes have the same phase speed. In particular, both upwind and central finite-volume methods maintain lagging phase error under exact time integration. Compared to the other methods examined in this paper they exhibit intermediate resolution of waves below fourth-order and poor resolution above fourth-order (see Figure 1), but consistently yield the largest stable Courant number (see Table 2), especially when taken to high-order.

Table 3. Schemes with no implicit diffusion: Shortest resolved wavenumber in the dispersive limit and diffusive limit, maximum stable Courant number and average number of non-zeros per node. These schemes include Central Finite-Volume (CFV) methods, Spectral Element Method (SEM), Modified Basis Spectral Element Method (MB-SEM) and Staggered Finite-Volume (stFV) method.

Scheme	Order	Shortest Resolved Wavelength		Maximum Stable Courant Number					Non-zeros
		Disp. Limit (Δx)		RK2	RK3	RK4	SSPRK53	SSPRK63	
CFV	2	16.01		-	1.73	2.83	2.69	3.06	4
	4	7.87		-	1.26	2.06	1.96	2.23	8
	6	5.80		-	1.09	1.78	1.70	1.93	12
	8	4.87		-	1.00	1.63	1.56	1.77	16
	10	4.34		-	0.94	1.54	1.47	1.66	20
SEM	2	16.01		-	1.73	2.83	2.69	3.07	4
	3	6.87		-	1.15	1.89	1.80	2.04	6
	4	8.40		-	0.95	1.55	1.48	1.68	8
	5	5.78		-	0.83	1.35	1.29	1.47	10
	6	4.82		-	0.74	1.21	1.15	1.31	12
	7	4.23		-	0.67	1.09	1.04	1.18	14
	8	5.43		-	0.60	0.99	0.94	1.07	16
	9	4.68		-	0.55	0.90	0.86	0.98	18
	10	4.25		-	0.51	0.83	0.79	0.90	20
	MB-SEM	4	4.32		-	0.95	1.56	1.48	1.69
5		3.36		-	0.85	1.39	1.32	1.50	10
6		4.12		-	0.78	1.28	1.22	1.39	12
7		3.82		-	0.74	1.21	1.15	1.31	14
8		3.52		-	0.71	1.15	1.10	1.25	16
stFV	2	10.08		-	0.87	1.41	1.35	1.53	4
	4	5.31		-	0.74	1.21	1.16	1.31	8
	6	4.13		-	0.70	1.14	1.09	1.24	12
	8	3.60		-	0.67	1.10	1.05	1.19	16
	10	3.30		-	0.66	1.07	1.02	1.16	20

Table 4. Coefficients of $A^{(\ell)}$ for upwind (central) finite-volume methods and $C^{(\ell)}$ for upwind finite-volume methods up to order 10.

Order	$A^{(-5)}$	$A^{(-4)}$	$A^{(-3)}$	$A^{(-2)}$	$A^{(-1)}$	$A^{(0)}$	$A^{(1)}$	$A^{(2)}$	$A^{(3)}$	$A^{(4)}$	$A^{(5)}$
1 (2)					$-\frac{1}{2}$	0	$\frac{1}{2}$				
3 (4)				$\frac{1}{12}$	$-\frac{2}{3}$	0	$\frac{2}{3}$	$-\frac{1}{12}$			
5 (6)			$-\frac{1}{60}$	$\frac{3}{20}$	$-\frac{3}{4}$	0	$\frac{3}{4}$	$-\frac{3}{20}$	$\frac{1}{60}$		
7 (8)		$\frac{1}{280}$	$-\frac{4}{105}$	$\frac{1}{5}$	$-\frac{4}{5}$	0	$\frac{4}{5}$	$-\frac{1}{5}$	$\frac{4}{105}$	$-\frac{1}{280}$	
9 (10)	$-\frac{1}{1260}$	$\frac{5}{504}$	$-\frac{5}{84}$	$\frac{5}{21}$	$-\frac{5}{6}$	0	$\frac{5}{6}$	$-\frac{5}{21}$	$\frac{5}{84}$	$-\frac{5}{504}$	$\frac{1}{1260}$

Order	$C^{(-5)}$	$C^{(-4)}$	$C^{(-3)}$	$C^{(-2)}$	$C^{(-1)}$	$C^{(0)}$	$C^{(1)}$	$C^{(2)}$	$C^{(3)}$	$C^{(4)}$	$C^{(5)}$
1					$\frac{1}{2}$	-1	$\frac{1}{2}$				
3				$-\frac{1}{12}$	$\frac{1}{3}$	$-\frac{1}{2}$	$\frac{1}{3}$	$-\frac{1}{12}$			
5			$\frac{1}{60}$	$-\frac{1}{10}$	$\frac{1}{4}$	$-\frac{1}{3}$	$\frac{1}{4}$	$-\frac{1}{10}$	$\frac{1}{60}$		
7		$-\frac{1}{280}$	$\frac{1}{35}$	$-\frac{1}{10}$	$\frac{1}{5}$	$-\frac{1}{4}$	$\frac{1}{5}$	$-\frac{1}{10}$	$\frac{1}{35}$	$-\frac{1}{280}$	
9	$\frac{1}{1260}$	$-\frac{1}{126}$	$\frac{1}{28}$	$-\frac{2}{21}$	$\frac{1}{6}$	$-\frac{1}{5}$	$\frac{1}{6}$	$-\frac{2}{21}$	$\frac{1}{28}$	$-\frac{1}{126}$	$\frac{1}{1260}$

3.2. Spectral Finite-Volume (SFV) methods

The spectral finite-volume method of Wang (2002) can be thought of as a high-order compact version of the

finite-volume method. An advection scheme on the cubed-sphere using this technique has been developed by Cheruvu *et al.* (2007) and a shallow water model was presented by Choi *et al.* (2004). Under the SFV framework the problem

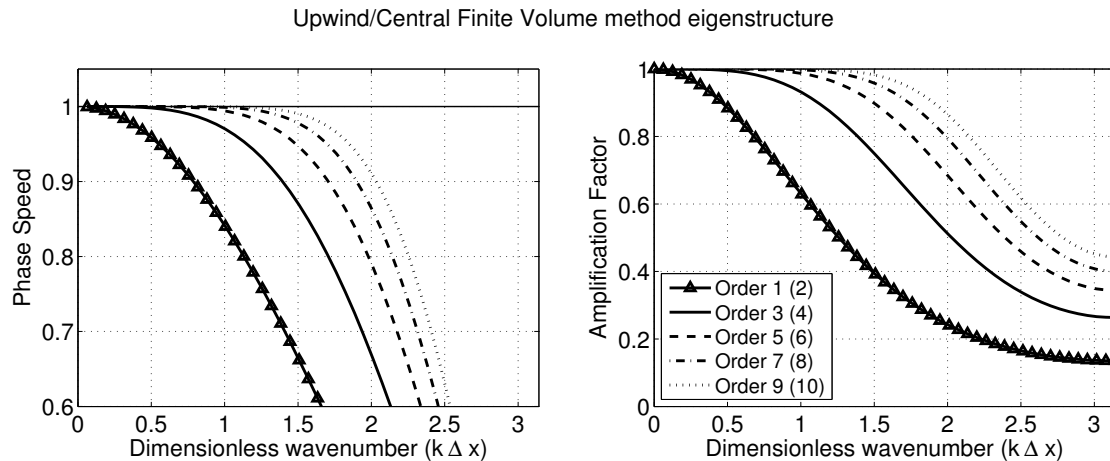


Figure 2. Phase speed and amplification factor of finite-volume methods up to ninth-order. Central finite-volume methods of even order p have the same phase speed of upwind finite-volume methods of order $p - 1$ and no amplification.

domain is first broken up into a set of *spectral volumes*. The spectral volumes are then broken up into a set of m *control volumes*, each of which has an associated element average (each element average then corresponds to a degree of freedom within the larger spectral volume). To evolve the flow, a polynomial is fit through all control volumes within a spectral volume to approximate the sub-grid-scale behavior of these fields. Since this fit is continuous within a spectral volume, fluxes are computed at interior edges by simple evaluation of the flux function. At spectral volume boundaries, fluxes are computed via a Riemann solver. The dispersive properties of this method have been investigated separately by [Van den Abeele et al. \(2007\)](#).

Note that the dispersive properties of the method are sensitive to the arrangement of control volumes, which in this paper are chosen to be bounded by Gaussian quadrature nodes. Surprisingly, this choice of control volumes leads to identical dispersive properties to the flux reconstruction method of [Huynh \(2007\)](#) with g_{Ga} correction function. Under this selection, the coefficients of SFV methods of order 2 and 3 are given in Table 5. The phase speed and amplification factor for SFV methods up to order 9 are depicted in Figure 3. Under exact integration, SFV methods have lagging phase error up to fourth-order and leading phase error at sixth-order and above. Due to the use of an upwind flux and compact stencil, these methods do not allow for spurious backward propagating wave modes. Comparing SFV against the other schemes in this paper indicates that they capture the phase speed very well at fifth-order and above, compare favorably in terms of their maximum stable Courant number and exhibit intermediate diffusion (see Figure 1). The fifth-order version of this method has the best phase capturing properties, whereas above fifth-order the dispersive limit actually stagnates, and improvements are only provided by weakening the effects of diffusion at longer wavelengths.

If a central flux is used at element boundaries in place of the Riemann solver, the $C^{(\ell)}$ matrices are zeroed. If a central flux is used and the edges of control volumes are placed at Gauss-Lobatto nodes, SFV then has the same dispersive properties as SEM.

3.3. Discontinuous Galerkin (DG) and Mass-Lumped DG (DG*) methods

DG methods are a cornerstone of high-order compact numerical methods ([Cockburn and Shu 1989](#); [Cockburn et al. 1990](#)). Although no operational dynamical core currently utilizes these methods, several experimental codes have been developed that use DG for transport, shallow-water and mesoscale modeling. The nodal formulation has been presented in its standard form (with exact mass matrix) on Gauss-Legendre (GL) nodes ([Giraldo et al. 2002](#); [Nair et al. 2005a,b](#)) and in its mass-lumped (or diagonalized mass matrix) form on Gauss-Legendre-Lobatto (GLL) nodes ([Giraldo and Rosmond 2004](#); [Dennis et al. 2006](#); [Giraldo and Restelli 2008](#)). However, regardless of whether a GL or GLL basis is chosen, these methods will have identical dispersion properties if exact integration is used for the mass matrix. This property further extends to all possible bases since the DG scheme can be defined in a basis-independent manner (see, for example, [Cotter and Ham \(2011, §3.2\)](#)). Both the discontinuous Galerkin method and mass-lumped discontinuous Galerkin method were also recovered by [Huynh \(2007\)](#) within the framework of flux correction schemes using the g_1 and g_2 correction functions, respectively. This paper examines the dispersive properties of DG with both an exact mass matrix and a diagonalized mass matrix. A similar detailed dispersion analysis has been performed by [Hu et al. \(1999\)](#) for both the exact mass matrix and with a central flux, in which case the dispersive properties closely match those of SEM. The dispersive properties of discontinuous Galerkin methods have also been analyzed in detail by [Sherwin \(2000\)](#).

In general, a DG method of order m stores m DOFs per element. The use of a Riemann solver leads to implicit numerical diffusion. Coefficients of the $A^{(\ell)}$ and $C^{(\ell)}$ matrices are given in Tables 6 and 7 for the exact (DG) and diagonalized mass (DG*) matrix approaches, respectively. In particular, the DG* approach has the weakest coupling to neighboring elements of all compact numerical methods, having exactly one non-zero entry among each of $A^{(-1)}$, $A^{(1)}$, $C^{(-1)}$ and $C^{(1)}$. The structure of the diffusive matrix $C^{(0)}$ highlights the need for additional diffusion within an

Table 5. Coefficients $A^{(\ell)}$ and $C^{(\ell)}$ for spectral volume methods up to order 3.

Order	$A^{(-1)}$	$A^{(0)}$	$A^{(1)}$
2	$\begin{pmatrix} \frac{1}{2} & -\frac{3}{2} \\ 0 & 0 \end{pmatrix}$	$\begin{pmatrix} -\frac{1}{2} & \frac{3}{2} \\ -\frac{3}{2} & \frac{1}{2} \end{pmatrix}$	$\begin{pmatrix} 0 & 0 \\ \frac{3}{2} & -\frac{1}{2} \end{pmatrix}$
3	$\begin{pmatrix} -\frac{1}{2} & -2 + \frac{3}{2}\sqrt{3} & -\frac{7}{2} \\ 0 & 0 & 0 \\ 0 & 0 & 0 \end{pmatrix}$	$\begin{pmatrix} -\frac{5}{2} + \sqrt{3} & -1 + \frac{3}{2}\sqrt{3} & \frac{1}{2} - \sqrt{3} \\ -2\sqrt{3} & 0 & 2\sqrt{3} \\ -\frac{1}{2} + \sqrt{3} & 1 - \frac{3}{2}\sqrt{3} & \frac{5}{2} - \sqrt{3} \end{pmatrix}$	$\begin{pmatrix} 0 & 0 & 0 \\ 0 & 0 & 0 \\ \frac{7}{2} & 2 - \frac{3}{2}\sqrt{3} & \frac{1}{2} \end{pmatrix}$

Order	$C^{(-1)}$	$C^{(0)}$	$C^{(1)}$
2	$\begin{pmatrix} -\frac{1}{2} & \frac{3}{2} \\ 0 & 0 \end{pmatrix}$	$\begin{pmatrix} -\frac{3}{2} & \frac{1}{2} \\ \frac{1}{2} & -\frac{3}{2} \end{pmatrix}$	$\begin{pmatrix} 0 & 0 \\ \frac{3}{2} & -\frac{1}{2} \end{pmatrix}$
3	$\begin{pmatrix} \frac{1}{2} & 2 - \frac{3}{2}\sqrt{3} & \frac{7}{2} \\ 0 & 0 & 0 \\ 0 & 0 & 0 \end{pmatrix}$	$\begin{pmatrix} -\frac{7}{2} & -2 + \frac{3}{2}\sqrt{3} & -\frac{1}{2} \\ 0 & 0 & 0 \\ -\frac{1}{2} & -2 + \frac{3}{2}\sqrt{3} & -\frac{7}{2} \end{pmatrix}$	$\begin{pmatrix} 0 & 0 & 0 \\ 0 & 0 & 0 \\ \frac{7}{2} & 2 - \frac{3}{2}\sqrt{3} & \frac{1}{2} \end{pmatrix}$

element (often provided by a Boyd-Vandeven filter (Boyd 1996), for example), since the basic form of this method does not admit intra-element diffusion. The phase speed and amplification factor for DG methods with an exact mass matrix are given in Figure 4 and with a diagonalized mass matrix in Figure 5. Like SFV methods, the upwind nature of this formulation implies that these methods do not allow for spurious backward propagating wave modes.

With the exact mass matrix, DG methods have a leading phase error and very strong diffusion at short wavelengths. Below fifth-order, these methods also have the best wave resolution among all methods with implicit diffusion but also have the most restrictive CFL condition (see Figure 1 and Table 2). With the diagonalized mass matrix, the phase error is lagging up to fifth-order and leading for sixth-order and above. Diffusion is much weaker with the diagonalized mass matrix and maximum phase speed significantly slower, and so the CFL condition for the diagonalized method is significantly more lenient (see Table 2). However, below fifth-order the errors associated with the diagonalized variant are also significantly larger, and consequently in this range this method has the worst resolved waves among competing schemes (see Figure 1). These results agree with the observations of Mullen and Belytschko (1982), who argue that mass lumping markedly increase the dispersive errors of the method. On the other hand, at fifth-order and above the picture changes dramatically and DG* has among the best resolved phase speeds.

If a central flux is used at element boundaries in place of the Lax-Friedrichs Riemann solver, the $C^{(\ell)}$ matrices are zeroed. In this case DG* methods with a central flux have equivalent dispersive properties to SEM.

3.4. Spectral Element Methods (SEM)

The spectral element method (Patera 1984; Maday and Patera 1989) has several important properties including parallel scalability, flexibility and accuracy, that make it a desirable choice for atmospheric dynamics. This approach was first adopted in the ocean modeling community by Ma (1993) and later for shallow water simulations on the sphere by Taylor *et al.* (1997). More recently, the spectral element method has been implemented as an atmospheric dynamical core (Fournier *et al.* 2004) and is now included as part of the Community Atmosphere Model (CAM) as the likely default dynamical core (Taylor and Fournier 2010; Dennis *et al.* 2012). A regional modeling environment using both the spectral element and discontinuous Galerkin method has also been developed (Giraldo and Rosmond 2004; Giraldo and Restelli 2008). SEM has been previously analyzed by Giraldo (1998), Ainsworth and Wajid (2009), and more recently by Melvin *et al.* (2012).

SEM can be formulated either as a finite-element method with a continuous and compact set of test functions and mass-lumped mass matrix, or as a conservative finite-difference method on a compact stencil. Both approaches lead to an identical formulation over an infinite or periodic domain. For a SEM of order $m + 1$, each spectral element stores m degrees of freedom per state variable, which are associated with nodal values at the Gauss-Lobatto quadrature nodes. This approach reduces to the central finite-volume approach at second-order, and has no corresponding first-order analogue. Coefficients of the evolution matrices for the 1D advection equation up to fourth-order accuracy are given in Table 8.

The shortest resolved wavelength for SEM up to tenth-order is given in Table 3. The erratic behavior associated with the shortest resolved wavelength of the spectral element method can be attributed to the ‘‘spectral gap’’,

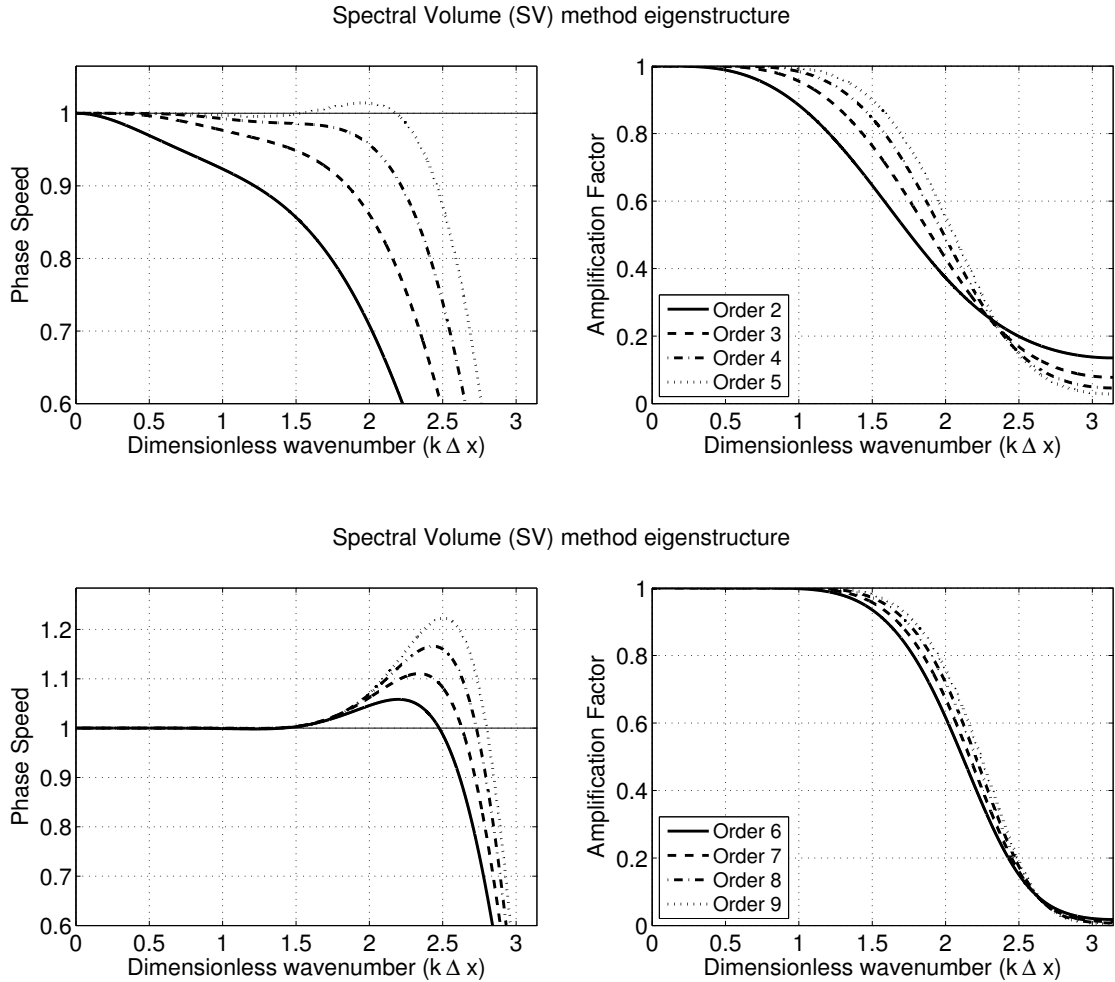


Figure 3. Phase speed and amplification factor of SFV methods up to ninth-order.

Table 6. Coefficients $A^{(\ell)}$ for the discontinuous Galerkin method (on GLL nodes without mass lumping) up to order 3.

Order	$A^{(-1)}$	$A^{(0)}$	$A^{(1)}$
2	$\begin{pmatrix} 0 & -2 \\ 0 & 1 \end{pmatrix}$	$\begin{pmatrix} 1 & 2 \\ -2 & -1 \end{pmatrix}$	$\begin{pmatrix} -1 & 0 \\ 2 & 0 \end{pmatrix}$
3	$\begin{pmatrix} 0 & 0 & -\frac{9}{2} \\ 0 & 0 & \frac{3}{4} \\ 0 & 0 & -\frac{3}{2} \end{pmatrix}$	$\begin{pmatrix} \frac{3}{2} & 4 & -\frac{5}{2} \\ -\frac{7}{4} & 0 & \frac{7}{4} \\ \frac{5}{2} & -4 & -\frac{3}{2} \end{pmatrix}$	$\begin{pmatrix} \frac{3}{2} & 0 & 0 \\ -\frac{3}{4} & 0 & 0 \\ \frac{9}{2} & 0 & 0 \end{pmatrix}$
Order	$C^{(-1)}$	$C^{(0)}$	$C^{(1)}$
2	$\begin{pmatrix} 0 & 2 \\ 0 & -1 \end{pmatrix}$	$\begin{pmatrix} -2 & 1 \\ 1 & -2 \end{pmatrix}$	$\begin{pmatrix} -1 & 0 \\ 2 & 0 \end{pmatrix}$
3	$\begin{pmatrix} 0 & 0 & \frac{9}{2} \\ 0 & 0 & -\frac{3}{4} \\ 0 & 0 & \frac{3}{2} \end{pmatrix}$	$\begin{pmatrix} -\frac{9}{2} & 0 & -\frac{3}{2} \\ \frac{3}{4} & 0 & \frac{3}{4} \\ -\frac{3}{2} & 0 & -\frac{9}{2} \end{pmatrix}$	$\begin{pmatrix} \frac{3}{2} & 0 & 0 \\ -\frac{3}{4} & 0 & 0 \\ \frac{9}{2} & 0 & 0 \end{pmatrix}$

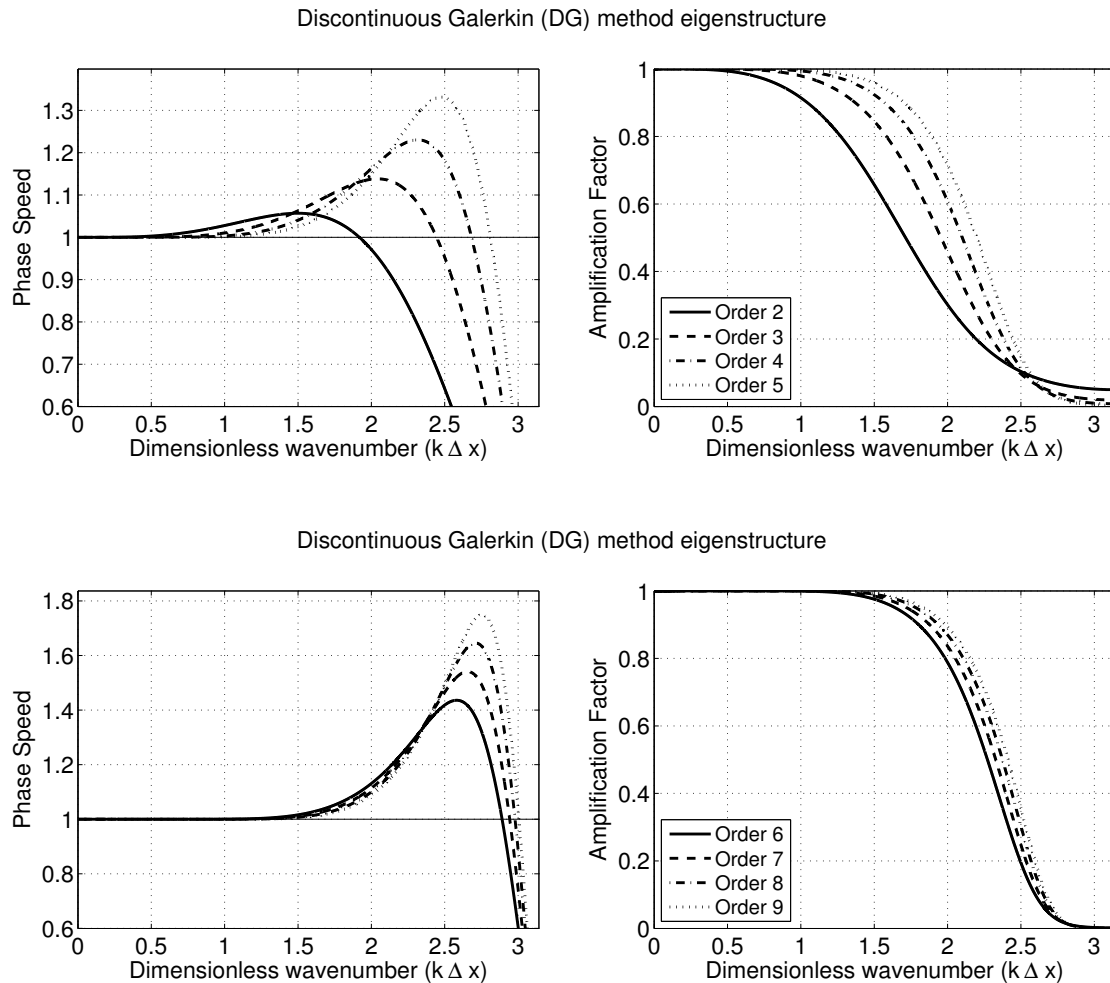


Figure 4. Phase speed and amplification factor of the discontinuous Galerkin (DG) method for up to ninth-order.

which is associated with an unphysical jump in the phase speed (see Figure 6). The spectral gap is a feature that arises among compact schemes, and is especially prominent when these schemes have either insufficient or zero diffusion. This difference arises when the natural modes of the discretization become increasingly divergent from sinusoids and become increasingly localized near element boundaries. The sinusoidal approximation to these localized eigenvectors is typically poor and tends to be discontinuous when transitioning from physical wave modes to numerical artifacts. Consequently, although SEM can have highly accurate dispersive properties at shorter wavelengths, the presence of the spectral gap leads to an early cutoff in the dispersive limit of this method. For instance, although the phase speed for $k\Delta x \in [1, 1.5]$ is fairly well captured for the fourth-order SEM (Figure 6), the shortest resolved wavelength is determined by the gap near $k\Delta x = 0.78$. It has been observed that the spectral gap can be effectively removed via the addition of explicit diffusion or, as described in the following section, by shifting the interior GLL nodes.

3.5. Modified Basis Spectral Element Methods (MB-SEM)

The spectral gap associated with SEM can be removed via an appropriate modified choice of basis functions. Under this approach Gauss-Lobatto quadrature points are abandoned, and instead the nodal basis points are chosen to avoid any jumps in the dispersion spectrum of the underlying method. To the best of the author's knowledge, this approach has not been studied elsewhere. The evolution equations are assembled using the finite-difference formulation, and so nodal weights are not required. Consequently, these restrictions lead to one remaining free parameter for the fourth- and fifth-order schemes, two remaining free parameters for the sixth- and seventh-order schemes, and so forth. Although the N nodal points within a spectral element (plus one shared node) can no longer be used for exact integration up to order $2N - 1$, the scheme nonetheless maintains order $N + 1$ accuracy on a uniform mesh.

As with the SEM method, MB-SEM is formulated to conserve linear wave energy exactly. The phase speed for waves under this approach is depicted in Figure 7 for formulations up to ninth-order. As observed in this figure, the modified basis method successfully removes the spectral

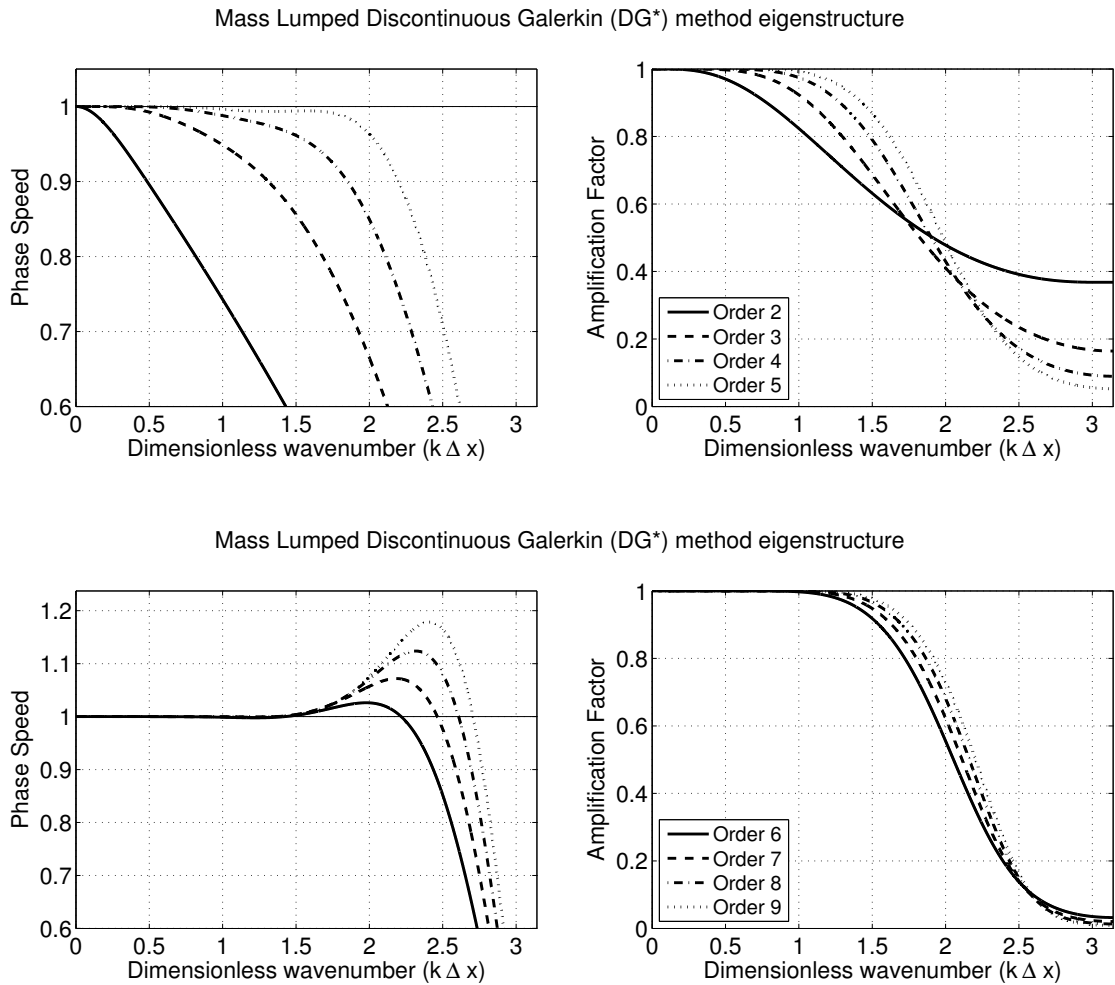


Figure 5. Phase speed and amplification factor of the mass-lumped discontinuous Galerkin (DG*) method for up to ninth-order.

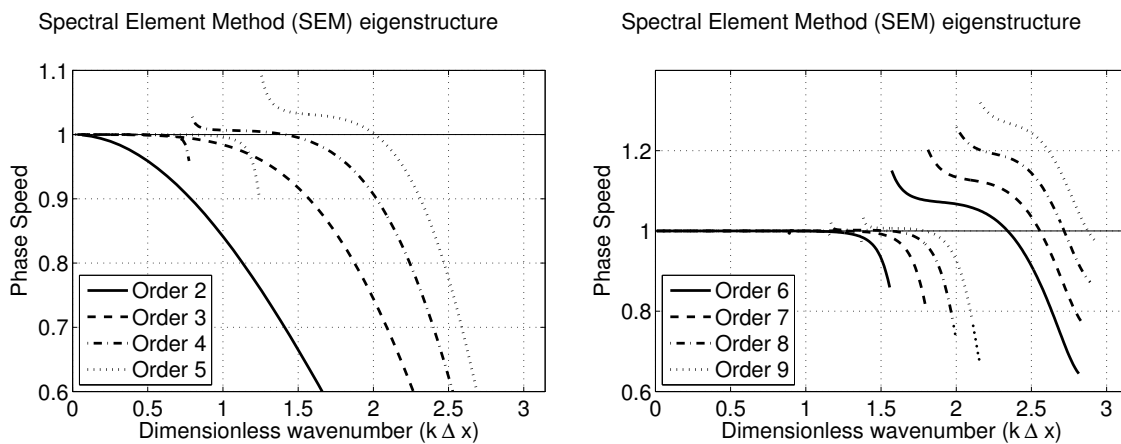


Figure 6. Phase speed of SEM up to ninth-order.

gap for the SEM and further improves the accuracy of the method. Further, as observed in Table 3, this approach also increases the maximum stable time step for the method, especially for formulations above fifth-order. The shortest resolved wavenumber of this approach is also the best of

all approaches studied in the paper, boasting resolution approaching $4\Delta x$ at only fourth-order accuracy.

Table 7. Coefficients $A^{(\ell)}$ for the discontinuous Galerkin method (on GLL nodes with mass lumping) up to order 4.

Order	$A^{(-1)}$	$A^{(0)}$	
2	$\begin{pmatrix} 0 & -1 \\ 0 & 0 \end{pmatrix}$	$\begin{pmatrix} 0 & 1 \\ -1 & 0 \end{pmatrix}$	$\begin{pmatrix} 0 & 0 \\ 1 & 0 \end{pmatrix}$
3	$\begin{pmatrix} 0 & 0 & -3 \\ 0 & 0 & 0 \\ 0 & 0 & 0 \end{pmatrix}$	$\begin{pmatrix} 0 & 4 & -1 \\ -1 & 0 & 1 \\ 1 & -4 & 0 \end{pmatrix}$	$\begin{pmatrix} 0 & 0 & 0 \\ 0 & 0 & 0 \\ 3 & 0 & 0 \end{pmatrix}$
4	$\begin{pmatrix} 0 & 0 & 0 & -6 \\ 0 & 0 & 0 & 0 \\ 0 & 0 & 0 & 0 \\ 0 & 0 & 0 & 0 \end{pmatrix}$	$\begin{pmatrix} 0 & \frac{5}{2}(1+\sqrt{5}) & \frac{5}{2}(1-\sqrt{5}) & 1 \\ -\frac{1}{2}(1+\sqrt{5}) & 0 & \sqrt{5} & \frac{1}{2}(1-\sqrt{5}) \\ -\frac{1}{2}(1-\sqrt{5}) & -\sqrt{5} & 0 & \frac{1}{2}(1+\sqrt{5}) \\ -1 & -\frac{5}{2}(1-\sqrt{5}) & -\frac{5}{2}(1+\sqrt{5}) & 0 \end{pmatrix}$	$\begin{pmatrix} 0 & 0 & 0 & 0 \\ 0 & 0 & 0 & 0 \\ 0 & 0 & 0 & 0 \\ 6 & 0 & 0 & 0 \end{pmatrix}$

Order	$C^{(-1)}$	$C^{(0)}$	$C^{(1)}$
2	$\begin{pmatrix} 0 & 1 \\ 0 & 0 \end{pmatrix}$	$\begin{pmatrix} -1 & 0 \\ 0 & -1 \end{pmatrix}$	$\begin{pmatrix} 0 & 0 \\ 1 & 0 \end{pmatrix}$
3	$\begin{pmatrix} 0 & 0 & 3 \\ 0 & 0 & 0 \\ 0 & 0 & 0 \end{pmatrix}$	$\begin{pmatrix} -3 & 0 & 0 \\ 0 & 0 & 0 \\ 0 & 0 & -3 \end{pmatrix}$	$\begin{pmatrix} 0 & 0 & 0 \\ 0 & 0 & 0 \\ 3 & 0 & 0 \end{pmatrix}$
4	$\begin{pmatrix} 0 & 0 & 0 & 6 \\ 0 & 0 & 0 & 0 \\ 0 & 0 & 0 & 0 \\ 0 & 0 & 0 & 0 \end{pmatrix}$	$\begin{pmatrix} -6 & 0 & 0 & 0 \\ 0 & 0 & 0 & 0 \\ 0 & 0 & 0 & 0 \\ 0 & 0 & 0 & -6 \end{pmatrix}$	$\begin{pmatrix} 0 & 0 & 0 & 0 \\ 0 & 0 & 0 & 0 \\ 0 & 0 & 0 & 0 \\ 6 & 0 & 0 & 0 \end{pmatrix}$

Table 8. Coefficients $A^{(\ell)}$ for the spectral element method up to order 4.

Order	$A^{(-1)}$	$A^{(0)}$	$A^{(1)}$
2	$\begin{pmatrix} -\frac{1}{2} \end{pmatrix}$	0	$\begin{pmatrix} \frac{1}{2} \end{pmatrix}$
3	$\begin{pmatrix} \frac{1}{2} & -2 \\ 0 & 0 \end{pmatrix}$	$\begin{pmatrix} 0 & 2 \\ -1 & 0 \end{pmatrix}$	$\begin{pmatrix} -\frac{1}{2} & 0 \\ 1 & 0 \end{pmatrix}$
4	$\begin{pmatrix} -\frac{1}{2} & -\frac{5}{4}(1-\sqrt{5}) & -\frac{5}{4}(1+\sqrt{5}) \\ 0 & 0 & 0 \\ 0 & 0 & 0 \end{pmatrix}$	$\begin{pmatrix} 0 & \frac{5}{4}(1+\sqrt{5}) & \frac{5}{4}(1-\sqrt{5}) \\ -\frac{1}{2}(1+\sqrt{5}) & 0 & \sqrt{5} \\ -\frac{1}{2}(1-\sqrt{5}) & -\sqrt{5} & 0 \end{pmatrix}$	$\begin{pmatrix} \frac{1}{2} & 0 & 0 \\ \frac{1}{2}(1-\sqrt{5}) & 0 & 0 \\ \frac{1}{2}(1+\sqrt{5}) & 0 & 0 \end{pmatrix}$

3.6. Staggered Finite-Volume (stFV) methods

Staggered methods have been an integral part of atmospheric modeling since the early work of Arakawa and Lamb (1977) introduced the second-order Arakawa C-grid staggered scheme. To extend this approach to higher-orders, a successively wider polynomial is fit through

neighboring Φ and u nodes and derivatives computed where needed. This approach is roughly equivalent to the use of Richardson extrapolation with successively larger stencils (Morinishi *et al.* 1998). Consequently, the evolution coefficients satisfy the criteria $B^{(\ell)} = A^{(\ell+1)}$. The coefficients for the stFV methods up to tenth-order are given in Table 10.

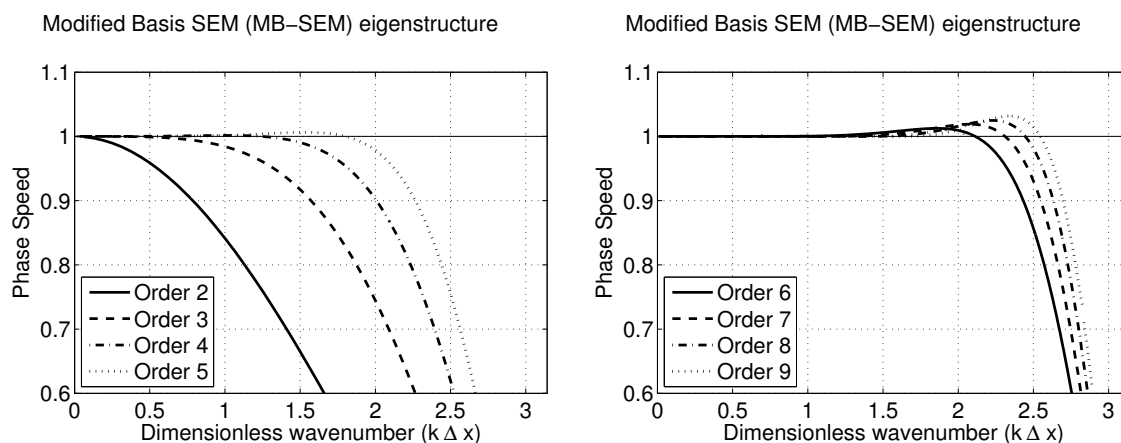


Figure 7. Phase speed of MB-SEM up to ninth-order.

Table 9. Nodal coordinates within a $[0, 1]$ reference element used for MB-SEM, obtained by a search over the space of all possible nodal coordinate values.

Order	ξ_2	ξ_3	ξ_4
4	0.2810046		
5	0.1839285		
6	0.1320270	0.3699272	
7	0.1006624	0.2875576	
8	0.0795166	0.2399534	0.3881677
9	0.0652070	0.1984990	0.3282781

As shown by Randall (1994), staggering of geopotential and velocity nodes greatly improves the dispersive properties of both the short- and long-wavelength scale as long as the grid spacing remains smaller than the Rossby radius of deformation (as is typically the case for modern climate models). These observations agree with the results in Figure 1, which show consistently strong performance for these methods. At second-order these methods have nearly twice the resolution of CFV methods, but also cost twice as much if run with the maximum stable Courant number (see Table 3). The higher-order variants of these methods also show rapid improvement in how well they handle wave-like motion. The phase speed for this class of methods is depicted in Figure 8; note that unlike the unstaggered methods that have been examined so far, staggered methods do not require zero phase speed when $k\Delta x = \pi$, and consequently tend to perform better for shorter waves.

As pointed out by Ullrich and Jablonowski (2011), staggered grid methods also tend to support physical wave reflection in the presence of grid refinement. This result is closely associated with the fact that $A^{(\ell)} \neq B^{(\ell)}$, and consequently the left-going and right-going Riemann invariants of the linearized shallow water equations do not decouple.

3.7. Other methods

The mixed finite-element approach (Raviart and Thomas 1977) is not addressed in this work, although this

method has experienced renewed interest for geophysical applications. Low-order finite-element methods and mixed finite-element methods on triangles have been analyzed by Foreman (1984); Le Roux *et al.* (1998); Hanert *et al.* (2004). In the context of atmospheric motions, mixed finite-element methods have more recently been analyzed by Staniforth *et al.* (2012).

Several second- and fourth-order numerical finite-difference methods have been analyzed by Sei and Symes (1995), using both a criteria related to accurate treatment of the dispersion relation and a measure of relative computational cost. Other numerical methods which have not been addressed in this work include the spectral difference method of Liu *et al.* (2006), the residual distribution method of Deconinck *et al.* (1993), the constrained interpolation profile scheme of Xiao (2004), the full set of flux recovery methods (Huynh 2007; Vincent *et al.* 2011) and the general class of characteristic-based methods (Norman *et al.* 2011).

4. Discussion and Intercomparison

The analysis procedure in this paper suggests an approach for answering the questions posed in section 1. Several other interesting results have also emerged from this analysis, many of which have been discussed in the context of specific numerical methods. This section now aims to address the comparative properties of each method.

One result from this work that may seem counter-intuitive is that, in the context of wave propagation, compact schemes emerge as competitive or better than similar non-compact methods. This result is of particular importance moving forward, since the growth of massively parallel supercomputers makes these methods particularly desirable (Dennis *et al.* 2012).

The questions posed earlier have also been addressed:

What are the shortest waves which can be considered “resolved” for a particular numerical method?

Ignoring effects due to explicitly imposed diffusion, Figure 1 and Tables 2-3 present the shortest resolved wavelength from several popular numerical methods at an error rate of $\tilde{e}_r = \tilde{e}_i = 0.01$. These results suggest that the

Table 10. Coefficients $A^{(\ell)}$ for the staggered finite-volume method up to order 10. The $B^{(\ell)}$ coefficients satisfy $B^{(\ell)} = A^{(\ell+1)}$.

Order	$A^{(-4)}$	$A^{(-3)}$	$A^{(-2)}$	$A^{(-1)}$	$A^{(0)}$	$A^{(1)}$	$A^{(2)}$	$A^{(3)}$	$A^{(4)}$	$A^{(5)}$
2					-1	1				
4				$\frac{1}{24}$	$-\frac{9}{8}$	$\frac{9}{8}$	$-\frac{1}{24}$			
6			$-\frac{3}{640}$	$\frac{25}{384}$	$-\frac{75}{64}$	$\frac{75}{64}$	$-\frac{25}{384}$	$\frac{3}{640}$		
8		$\frac{5}{7168}$	$-\frac{49}{5120}$	$\frac{245}{3072}$	$-\frac{1225}{1024}$	$\frac{1225}{1024}$	$-\frac{245}{3072}$	$\frac{49}{5120}$	$-\frac{5}{7168}$	
10	$-\frac{35}{294912}$	$\frac{405}{229376}$	$-\frac{567}{40960}$	$\frac{735}{8192}$	$-\frac{19845}{16384}$	$\frac{19845}{16384}$	$-\frac{735}{8192}$	$\frac{567}{40960}$	$-\frac{405}{229376}$	$\frac{35}{294912}$

Staggered Finite Volume method eigenstructure

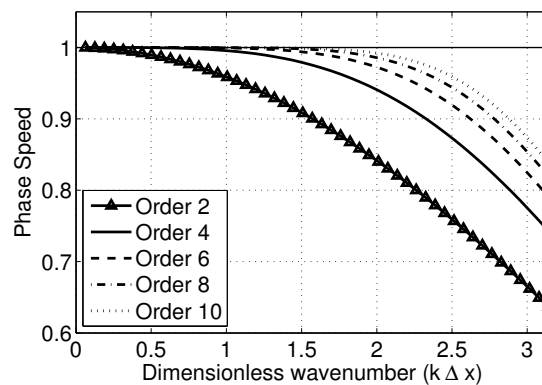


Figure 8. Phase speed and amplification factor of stFV methods up to tenth-order.

shortest resolved wavelength for many operational models is $8\Delta x$ or longer. In fact, the current generation of models largely fall short of the shortest resolved wavelength of $4\Delta x$ which is frequently posited for these methods. A shortest resolved wavelength at this level is only reached by DG, MB-SEM and stFV.

Note that the strong falloff of the phase speed and amplification factor as a function of $k\Delta x$ for these methods implies variations in the error level will not lead to significantly different results for the shortest resolved wavelength. For example, for many of the fourth-order methods discussed in this paper, an error level of $\tilde{\epsilon}_r = \tilde{\epsilon}_i = 0.1$ is needed in order for waves at $4\Delta x$ to be considered resolved. For reference, this error level is ten times larger than the reference value chosen in this paper, corresponding to complete phase reversal over a distance of $(\pi/0.1)\Delta x$ and 65% damping over a distance of $10\Delta x$.

Examining Table 2, it is clear that the shortest resolved wavelength predicted by methods with implicit diffusion is determined almost exclusively by diffusive errors (except for the highest order DG methods). This result can be either taken to suggest that methods with implicit diffusion are overly-diffusive, or that the error level $\tilde{\epsilon}_i = 0.01$ is an overly strict requirement. To answer this question, it is necessary to study the non-linear equations to understand how much diffusion is necessary to prevent an accumulation of enstrophy at the shortest scales.

What is the effect of increasing the order of accuracy of a numerical discretization on its treatment of waves?

From Figure 1, it is clear that although increasing the order of accuracy of numerical methods does typically reduce the shortest resolved wavelength of these methods, there appears to be diminishing returns above fourth-order accuracy. On the other end of the spectrum, second-order methods seem insufficient to even provide resolution above $10\Delta x$. Consequently, there is a “sweet spot” around fourth-order accuracy where most numerical methods provide the desired accuracy without an overly strict restriction on the Courant number.

For a given order of accuracy, which numerical methods offer the best treatment of wave-like motion?

For purposes of intercomparison, schemes with and without implicit diffusion are considered separately. Among schemes with implicit diffusion, DG methods offer the best overall resolution, but also have the most restrictive CFL condition. SFV and DG* generally perform poorly below fifth-order, but at fifth-order and higher have the best representation of the phase speed among all competing methods. Among schemes without implicit diffusion, the presence of the spectral gap appears to severely damage the dispersive properties of SEM above third-order. If the SEM

basis is modified by adjusting the location of nodal points to obtain MB-SEM, the resulting approach has the best dispersive properties among all other competing methods. Staggering the grid, as with the stFV method, yields a very accurate dispersion relation at second-order, but this approach is still outperformed by any third-order or higher unstaggered method.

For a given error level, which numerical method and order of accuracy is the most computationally efficient?

For a fixed error level (and variable grid resolution), Figure 9 shows the approximate equal error cost (31) computed from Tables 2-3 for RK4 and SSPRK53 time integration. Among schemes with implicit diffusion, the DG* method, with its weak inter-nodal coupling, is the clear winner. On the other hand, DG with its highly restrictive CFL condition, is the most costly of these methods. Both SFV and UFV sit somewhere between these two methods in terms of cost. However, all four of these methods exhibit minimum approximate equal error cost at third-order accuracy. Comparing time-integrators, SSPRK53 yields a lower overall cost for SFV, DG and DG*, whereas RK4 is more efficient for UFV. Among schemes with no implicit diffusion, SEM provides the lowest cost, again at third-order accuracy. However, the minimum of the cost curve is less clear than for methods with implicit diffusion. All schemes exhibit a monotone increase of approximate equal error cost with order of accuracy above fourth-order.

It should be noted that approximate equal error cost does not necessarily apply in 2D or higher, where the expense of increased grid resolution can quickly outweigh other cost factors. In this case, methods higher than third-order (with longer resolved wavelengths) are more likely yield minimum cost. This topic will be tackled in a following paper.

5. Conclusions

This paper has presented a framework for intercomparison of the dispersive and diffusion properties of numerical methods for the 1D linearized shallow water equations without Coriolis term. This investigation aimed to determine the effective resolution of eight numerical methods, in terms of the shortest wavelength which could be considered to be well resolved. Such an approach to better understanding these methods is arguably more relevant to studies of atmospheric motion (where wave motion is the dominant feature) than convergence studies for instance, which emphasize the longest, already resolved wave modes. Implementations of these methods from first-order accuracy to tenth-order accuracy were examined. To the best of the author's knowledge, this is the first paper to provide an intercomparison of dispersive properties over many classes of numerical methods (compact, non-compact, staggered, with and without implicit diffusion).

Several observations have emerged from this analysis related to specific numerical methods. For non-compact schemes it was shown that the dispersive and diffusive properties of the method were decoupled when these operators were applied in an operator split manner. The use of mass-lumping of the DG method was explored, and although the mass-lumped DG method significantly weakened the CFL condition, it also led to an increase in the strength of implicit diffusion at long wavelengths

and led to greater inaccuracy in the phase speed for methods below fifth-order. The spectral gap present in SEM led to erratic behavior under the criteria explored in this work. To combat this problem MB-SEM was introduced as a spectral element-based approach which removed the spectral gap by making an adjustment to the interior nodal points. This modified method provided outstanding dispersion properties and actually improved on the CFL condition of SEM. It was also verified that staggering of the geopotential and velocity greatly improves the dispersive properties of the underlying method, although the second-order staggered scheme underperforms any third-order or higher unstaggered scheme, and consequently is not recommended.

In addition, several general observations were made that seem to be applicable across all of the numerical methods investigated. Perhaps most importantly, it was verified that compact methods are competitive with non-compact methods for resolution of waves. At the error level used in this paper ($\bar{\epsilon}_r = \bar{\epsilon}_i = 0.01$) it was also observed that numerical methods of fourth-order accuracy or higher were the absolute minimum for resolving waves near $4\Delta x$. However, it also emerged that the ability of many of these numerical methods to correctly capture waves does not seem to significantly improve above fifth-order accuracy. Since the CFL condition for these methods (compact schemes, in particular) leads to a rapid decrease in maximum stable Courant number with order of accuracy, it seems evident that there is a "sweet spot" between third- and fifth-order where resolution and cost are balanced. In fact, computing the approximate equal error cost of each of these methods suggested that third-order accuracy provided optimal efficiency, as long as grid resolution was allowed to vary.

This paper is a first step in better understanding how well numerical methods capture the wave-like nature of geophysical phenomena. Moving forward, several topics remain to be examined, including how the addition of explicit diffusion influences the numerical phase speed, how this analysis can be extended to the case of inexact time integration, and what effect fully implicit time discretizations have on the ability of these methods to accurately capture waves. Most importantly, this analysis will be extended to the 1D and 2D shallow water equations to better understand how well they are able to capture shallow-water wave modes in the presence of Coriolis forcing.

Acknowledgement

The author gratefully acknowledge helpful discussions during the course of this work with Peter Lauritzen, Hans Johansen, Francis Giraldo and James Kent. This work was supported by the University of California Davis.

References

- Ainsworth M, Wajid H. 2009. Dispersive and dissipative behavior of the spectral element method. *SIAM J. Numer. Anal.* **47**(5): 3910–3937.
- Arakawa A, Lamb V. 1977. Computational design and the basic dynamical processes of the UCLA general circulation model. *Meth. Comp. Phys.* **17**: 173–265.
- Boyd J. 1996. The erfc-log filter and the asymptotics of the Euler and Vandeven sequence accelerations. In: *Proceedings of the Third International Conference on Spectral and High Order Methods*, Ilin A V SLR (ed). pp. 267–276. Houston, Journal of Mathematics, Houston, Texas.

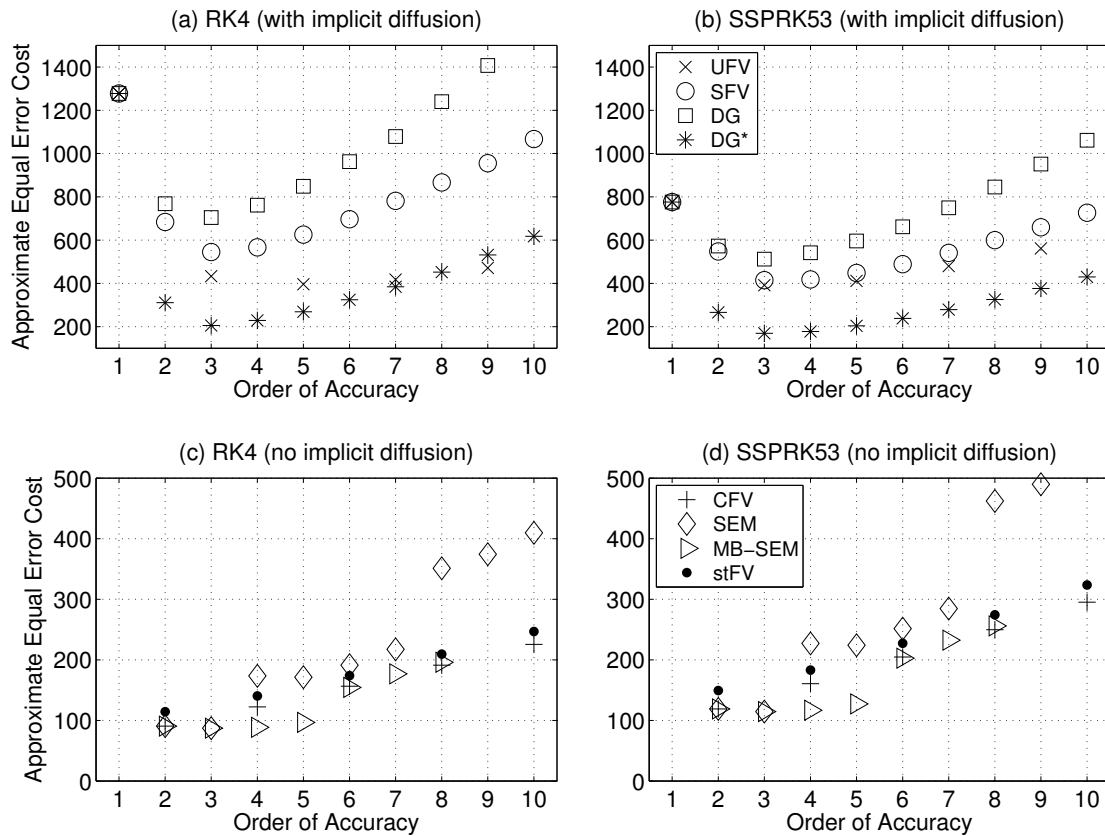


Figure 9. Approximate equal error cost of methods with implicit diffusion under (a) RK4 and (b) SSPRK53 time integrators and methods without implicit diffusion under (c) RK4 and (d) SSPRK53 time integrators with error level $\tilde{\epsilon}_r = \tilde{\epsilon}_i = 0.01$ for order of accuracy ≥ 1 . Among methods with implicit diffusion, the diffusive limit determines the shortest resolved wave in all cases except for DG methods of order ≥ 8 .

- Cheruvu V, Nair RD, Tufo HM. 2007. A spectral finite volume transport scheme on the cubed-sphere. *Appl. Numer. Math.* **57**(9): 1021–1032.
- Choi B, Iskandarani M, Levin J, Haidvogel D. 2004. A spectral finite-volume method for the shallow water equations. *Mon. Weather Rev.* **132**(7): 1777–1791.
- Cockburn B, Hou S, Shu C. 1990. The Runge-Kutta local projection discontinuous Galerkin finite element method for conservation laws IV: The multidimensional case. *Math. Comp.* **54**(190): 545–581.
- Cockburn B, Shu C. 1989. TVB Runge-Kutta local projection discontinuous Galerkin finite element method for conservation laws II: General framework. *Math. Comp.* **52**(186): 411–435.
- Colella P, Woodward PR. 1984. The Piecewise Parabolic Method (PPM) for gas-dynamical simulations. *J. Comput. Phys.* **54**: 174–201, doi:10.1016/0021-9991(84)90143-8.
- Cotter C, Ham D. 2011. Numerical wave propagation for the triangular $p_{DG}^1 - p^2$ finite element pair. *J. Comput. Phys.* **230**(8): 2806–2820.
- Deconinck H, Roe P, Struijs R. 1993. A multidimensional generalization of Roe's flux difference splitter for the Euler equations. *Computers & Fluids* **22**(2): 215–222.
- Dennis J, Edwards J, Evans K, Guba O, Lauritzen P, Mirin A, St-Cyr A, Taylor M, Worley P. 2012. CAM-SE: A scalable spectral element dynamical core for the Community Atmosphere Model. *Int. J. High Perform. Comput. Appl.* **26**(1): 74–89.
- Dennis JM, Nair RD, Tufo HM, Levy M, Voran T. 2006. Development of a scalable global discontinuous Galerkin atmospheric model. *Int. J. Comput. Sci. Eng* 11 pp.
- Foreman M. 1984. A two-dimensional dispersion analysis of selected methods for solving the linearized shallow water equations. *J. Comput. Phys.* **56**(2): 287–323.
- Fournier A, Taylor MA, Tribbia JJ. 2004. The Spectral Element Atmosphere Model (SEAM): High-resolution parallel computation and localized resolution of regional dynamics. *Mon. Weather Rev.* **132**(3): 726–748, doi:10.1175/1520-0493(2004)132<0726:TSEAMS>2.0.CO;2.
- Frederiksen J, Davies A. 1997. Eddy viscosity and stochastic backscatter parameterizations on the sphere for atmospheric circulation models. *J. Atmos. Sci.* **54**(20): 2475–2492.
- Giraldo FX. 1998. The Lagrange–Galerkin spectral element method on unstructured quadrilateral grids. *J. Comput. Phys.* **147**(1): 114–146.
- Giraldo FX, Hesthaven JS, Warburton T. 2002. Nodal high-order discontinuous Galerkin methods for the spherical shallow water equations. *J. Comput. Phys.* **181**(2): 499–525.
- Giraldo FX, Restelli M. 2008. A study of spectral element and discontinuous Galerkin methods for the Navier-Stokes equations in nonhydrostatic mesoscale atmospheric modeling: Equation sets and test cases. *J. Comput. Phys.* **227**: 3849–3877, doi:10.1016/j.jcp.2007.12.009.
- Giraldo FX, Rosmond TE. 2004. A Scalable Spectral Element Eulerian Atmospheric Model (SEE-AM) for NWP: Dynamical core tests. *Mon. Weather Rev.* **132**: 133–153, doi:10.1175/1520-0493(2004)132<0133:ASSEEA>2.0.CO;2.
- Godunov SK. 1959. A difference scheme for numerical solution of discontinuous solution of hydrodynamic equations. *Math. Sbornik* **47**: 271–306. Translated US Joint Publ. Res. Service, JPRS 7226, 1969.
- Hanert E, Le Roux D, Legat V, Deleersnijder E. 2004. Advection schemes for unstructured grid ocean modelling. *Ocean Modelling* **7**(1): 39–58.
- Harten A, Lax P, Van Leer B. 1983. On upstream differencing and Godunov-type schemes for hyperbolic conservation laws. *SIAM Review* **25**(1): 35–61.
- Hu FQ, Hussaini M, Rasetarinera P. 1999. An analysis of the discontinuous Galerkin method for wave propagation problems. *J. Comput. Phys.* **151**(2): 921–946, doi:10.1006/jcph.1999.6227.
- Huynh H. 2007. A flux reconstruction approach to high-order schemes including discontinuous Galerkin methods. *AIAA paper* **4079**.

- Lauritzen P. 2007. A stability analysis of finite-volume advection schemes permitting long time steps. *Mon. Weather Rev.* **135**(7): 2658–2673.
- Lauritzen PH, Jablonowski C, Taylor MA, Nair RD. 2010. Rotated versions of the Jablonowski steady-state and baroclinic wave test cases: A dynamical core intercomparison. *J. Adv. Model. Earth Sys.* **2**(4).
- Le Roux D, Staniforth A, Lin C. 1998. Finite elements for shallow-water equation ocean models. *Mon. Weather Rev.* **126**(7): 1931–1951.
- Li Y. 1997. Wavenumber-extended high-order upwind-biased finite-difference schemes for convective scalar transport. *J. Comput. Phys.* **133**(2): 235 – 255, doi:10.1006/jcph.1997.5649.
- Liu Y, Vinokur M, Wang Z. 2006. Spectral difference method for unstructured grids I: Basic formulation. *J. Comput. Phys.* **216**(2): 780–801.
- Ma H. 1993. A spectral element basin model for the shallow water equations. *J. Comput. Phys.* **109**: 133–149, doi:10.1006/jcph.1993.1205.
- Maday Y, Patera AT. 1989. Spectral element methods for the incompressible Navier-Stokes equations. In: *State-of-the-art surveys on computational mechanics (A90-47176 21-64)*. New York, American Society of Mechanical Engineers, 1989, p. 71–143. Research supported by DARPA. pp. 71–143.
- Melvin T, Staniforth A, Thuburn J. 2012. Dispersion analysis of the spectral element method. *Quart. J. Royal Meteor. Soc.* **138**(668): 1934–1947, doi:10.1002/qj.1906.
- Morinishi Y, Lund T, Vasilyev O, Moin P. 1998. Fully conservative higher order finite difference schemes for incompressible flow. *J. Comput. Phys.* **143**(1): 90 – 124, doi:10.1006/jcph.1998.5962, URL <http://www.sciencedirect.com/science/article/pii/S0021999198959629>.
- Mullen R, Belytschko T. 1982. Dispersion analysis of finite element semidiscretizations of the two-dimensional wave equation. *Int. J. Numer. Meth. Eng.* **18**(1): 11–29, doi:10.1002/nme.1620180103.
- Nair RD, Thomas S, Loft R. 2005a. A discontinuous Galerkin transport scheme on the cubed sphere. *Mon. Weather Rev.* **133**(4): 814–828.
- Nair RD, Thomas SJ, Loft RD. 2005b. A discontinuous Galerkin global shallow water model. *Mon. Weather Rev.* **133**(4): 876–888.
- Norman MR, Nair RD, Semazzi FH. 2011. A low communication and large time step explicit finite-volume solver for non-hydrostatic atmospheric dynamics. *J. Comput. Phys.* **230**(4): 1567 – 1584, doi: 10.1016/j.jcp.2010.11.022.
- Patera AT. 1984. A spectral element method for fluid dynamics: Laminar flow in a channel expansion. *J. Comput. Phys.* **54**(3): 468 – 488, doi: 10.1016/0021-9991(84)90128-1.
- Rančić M, Zhang H, Savic-Jovcic V. 2008. Nonlinear advection schemes on the octagonal grid. *Mon. Weather Rev.* **136**(12): 4668–4686.
- Randall D. 1994. Geostrophic adjustment and the finite-difference shallow-water equations. *Mon. Weather Rev.* **122**(6): 1371–1377.
- Raviart P, Thomas J. 1977. A mixed finite element method for 2-nd order elliptic problems. In: *Mathematical aspects of finite element methods*, Springer, pp. 292–315.
- Roe PL. 1981. Approximate Riemann solvers, parameter vectors, and difference schemes. *J. Comput. Phys.* **43**: 357–372, doi:10.1016/0021-9991(81)90128-5.
- Rossmannith JA. 2006. A wave propagation method for hyperbolic systems on the sphere. *J. Comput. Phys.* **213**: 629–658, doi:10.1016/j.jcp.2005.08.027.
- Ruuth S. 2006. Global optimization of explicit strong-stability-preserving Runge-Kutta methods. *Math. Comput.* **75**(253): 183–208.
- Sei A, Symes W. 1995. Dispersion analysis of numerical wave propagation and its computational consequences. *SIAM J. Sci. Comput.* **10**(1): 1–27.
- Sherwin S. 2000. Dispersion analysis of the continuous and discontinuous Galerkin formulations. In: *Discontinuous Galerkin Methods*, Springer, pp. 425–431.
- Skamarock W. 2008. A linear analysis of the NCAR CCSM finite-volume dynamical core. *Mon. Weather Rev.* **136**(6): 2112–2119.
- Staniforth A, Melvin T, Cotter C. 2012. Analysis of a mixed finite-element pair proposed for an atmospheric dynamical core. *Quart. J. Royal Meteor. Soc.* doi:10.1002/qj.2028.
- Taylor M, Tribbia J, Iskandarani M. 1997. The Spectral Element Method for the Shallow Water Equations on the Sphere. *J. Comput. Phys.* **130**: 92–108, doi:10.1006/jcph.1996.5554.
- Taylor MA, Fournier A. 2010. A compatible and conservative spectral element method on unstructured grids. *J. Comput. Phys.* **229**(17): 5879 – 5895, doi:10.1016/j.jcp.2010.04.008.
- Thuburn J. 2008. Numerical wave propagation on the hexagonal C-grid. *J. Comput. Phys.* **227**(11): 5836–5858.
- Thuburn J. 2011. Some basic dynamics relevant to the design of atmospheric model dynamical cores. In: *Numerical Techniques for Global Atmospheric Models*, Lauritzen PH, Jablonowski C, Taylor MA, Nair R (eds), Springer, pp. 3–27.
- Thuburn J, Ringler T, Skamarock W, Klemp J. 2009. Numerical representation of geostrophic modes on arbitrarily structured C-grids. *J. Comput. Phys.* **228**(22): 8321–8335.
- Ullrich P, Jablonowski C. 2011. An analysis of 1D finite-volume methods for geophysical problems on refined grids. *J. Comput. Phys.* **230**(3): 706–725.
- Ullrich PA, Jablonowski C. 2012a. MCore: A non-hydrostatic atmospheric dynamical core utilizing high-order finite-volume methods. *J. Comput. Phys.* **231**: 5078–5108, doi:10.1016/j.jcp.2012.04.024.
- Ullrich PA, Jablonowski C. 2012b. Operator-split Runge-Kutta-Rosenbrock methods for non-hydrostatic atmospheric models. *Mon. Weather Rev.* **140**: 1257–1284.
- Ullrich PA, Jablonowski CJ, van Leer BL. 2010. High-order finite-volume models for the shallow-water equations on the sphere. *J. Comput. Phys.* **229**: 6104–6134.
- Van den Abeele K, Broeckhoven T, Lacor C. 2007. Dispersion and dissipation properties of the 1D spectral volume method and application to a p-multigrid algorithm. *J. Comput. Phys.* **224**(2): 616 – 636, doi:10.1016/j.jcp.2006.10.022.
- Van Leer B. 1979. Towards the ultimate conservative difference scheme V - A second-order sequel to Godunov's method. *J. Comput. Phys.* **32**: 101–136, doi:10.1016/0021-9991(79)90145-1.
- Vincent P, Castonguay P, Jameson A. 2011. A new class of high-order energy stable flux reconstruction schemes. *J. Sci. Comp.* **47**(1): 50–72.
- Wang ZJ. 2002. Spectral (Finite) Volume Method for Conservation Laws on Unstructured Grids. Basic Formulation: Basic Formulation. *J. Comput. Phys.* **178**(1): 210 – 251, doi:10.1006/jcph.2002.7041.
- Xiao F. 2004. Unified formulation for compressible and incompressible flows by using multi-integrated moments I: One-dimensional inviscid compressible flow. *J. Comput. Phys.* **195**(2): 629–654.